Lockheed
Missiles & Space Company
Huntsville Research & Engineering Center
4800 Bradford Drive, Huntsville, AL 35807

Lockheed
Missiles & Space Company, Inc
Huntsville Research & Engineering Center
Cummings Research Park
4800 Bradford Drive
Huntsville, AL 35807

SPACE SHUTTLE MAIN ENGINE, POWERHEAD STRUCTURAL MODELING, STRESS AND FATIGUE LIFE ANALYSIS

VOLUME IV — SUMMARY OF INVESTIGATION OF UNSCHEDULED EVENTS AND SPECIAL TASKS

December 1983

Contract NAS8-34978

Prepared for National Aeronautics and Space Administration
Marshall Space Flight Center, AL 35812

by

J.K. Robinson
G.A. Teal
C.T. Welch

APPROVED C.T. Welch

C.T. Welch, Manager (Acting)
Product Engineering & Development Section

S.V. Bourgeois
Director

FOREWORD

This report summarizes the results of work performed on Contract NAS8-34978. The work was performed by personnel of the Product Engineering & Development Section of Lockheed's Huntsville Research & Engineering Center, for the National Aeronautics and Space Administration, George C. Marshall Space Flight Center, Alabama. The Contracting Officer's technical representative for this study is Mr. Norman C. Schlemmer, Structures and Propulsion Laboratory, Engineering Analysis Division, Stress Analysis Branch (EP46).

This report is divided into four volumes with a section covering one aspect of analysis for all components and loads, and a fourth section for investigation of unscheduled events and special tasks undertaken during the effort. The volumes are:

Volume I - Gasdynamic Environment of the SSME HPFTP and HPOTP Turbines, LMSC-HREC TR D867333-I.

Volume II - Dynamics of Blades and Nozzles - SSME HPFTP and HPOTP, LMSC-HREC TR D867333-II.

Volume III - Stress Summary of Blades and Nozzles at FPL and 115 percent RPL Loads SSME HPFTP and HPOTP Blades and Nozzles, LMSC-HREC TR D867333-III.

Volume IV - Summary of Investigation of Unscheduled Events and Special Tasks, LMSC-HREC TR D867333-IV.

It should be noted that this report summarized our findings. A great body of data exists in the form of computer printout and magnetic tapes and is available to any interested reader for either amplification of the summarized data or as a basis for further work.

CONTENTS

1. INTRODUCTION

This report contains a summary of the analyses performed for unscheduled events and special tasks which occurred during the contract period. These data have been presented to NASA-MSFC personnel as each task was completed. These presentations consisted of oral reviews and informal documentation.

2. LOW PRESSURE FUEL TURBOPUMP TURBINE LABYRINTH SEAL TIP RUBBING ANALYSIS

Teardown examination of the Low Pressure Fuel Turbopump (LPFTP) has shown evidence of rubbing occurring between the turbine inlet nozzle assembly and the labyrinth seal located on the first row turbine rotor assembly (Fig. 2-1). The pattern of rubbing is not constant around the circumference of the nozzle-labyrinth seal interface, and changing the configuration of the nozzle blockages has resulted in different rubbing patterns. Analysis was undertaken to isolate the cause of this rubbing and to show a correlation between rubbing patterns and nozzle blockage configuration.

The analysis focused on several particular components of the LPFTP which were identified as possible sources of the displacement or deformation necessary to close the allowable labyrinth seal gap. Finite element NASTRAN models of the selected components were constructed and analyzed using the appropriate computed pressures, temperatures, centrifugal loads, and dynamic loads. A summary of the analytical procedure as well as results for each component under consideration follows.

2.1 BEARING CARRIER

The variation in temperature between the bearing outer race and the bearing carrier has been speculated to allow a gap to open between the two parts allowing the turbine shaft to move freely in a radial direction. Assuming the shaft is cantilevered from the impeller end, the radial clearance at the bearing carrier would allow a corresponding deflection at the turbine end labyrinth seal.

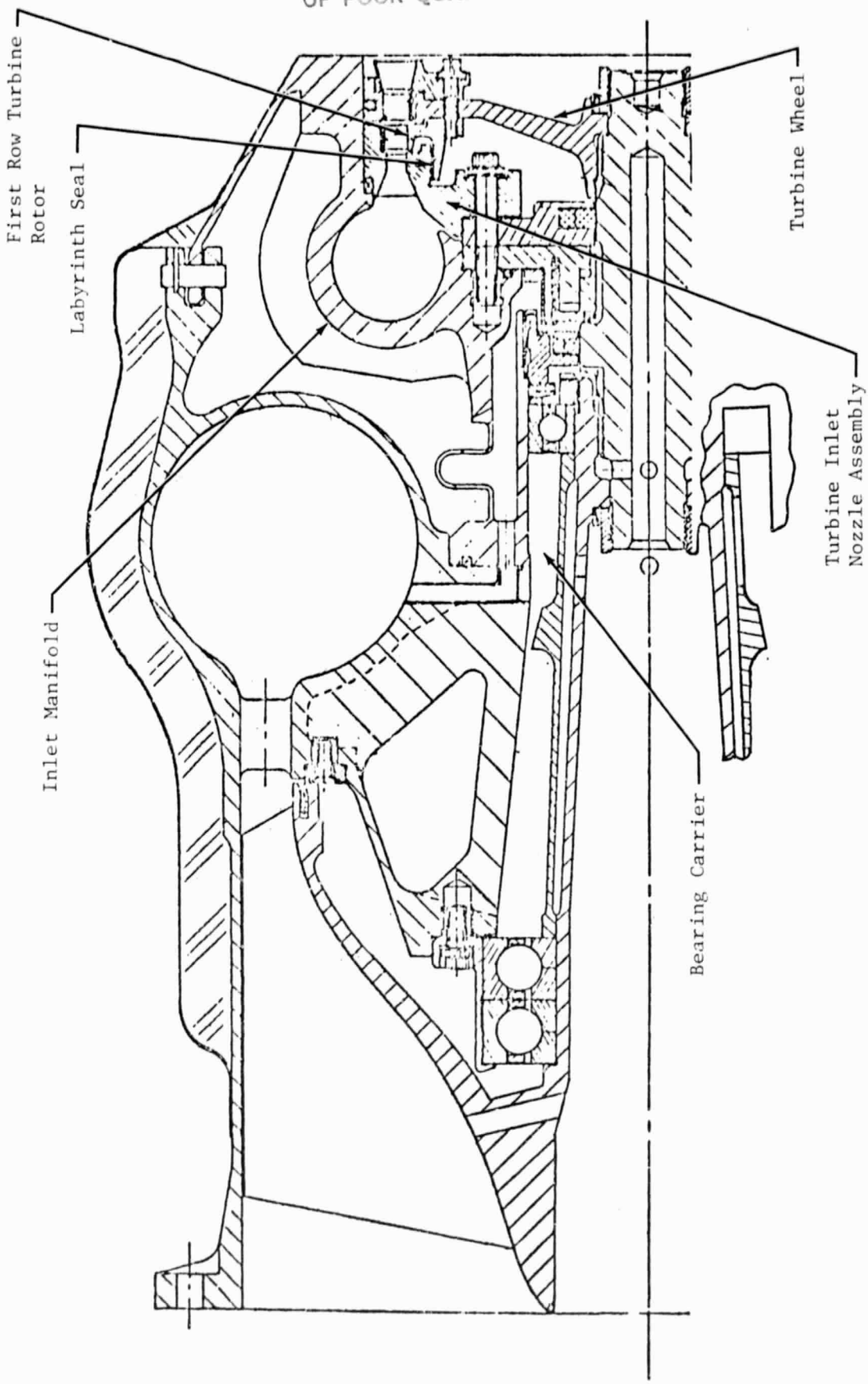

Fig. 2-1 Low Pressure Fuel Turbopump

The thermal and pressure loads shown in Fig. 2-2 were applied to the NASTRAN bearing carrier model (Fig. 2-3) while the bearing race thermal deformation was calculated by hand. The resulting radial deformations were combined to produce a maximum radial clearnace of .0038 in. Extrapolating the computed clearance axially to the labyrinth seal location yields a deflection of .0058 in.

2.2 TURBINE WHEEL AND FIRST ROW TURBINE ROTOR

The major sources of loading for the turbine wheel and rotors are centrifugal loads, pressure loads, and dynamic loads. The loading due to the high speed rotation and the pressure differential across the turbine disk is constant, while the turbine blades passing in and out of blocked inlet nozzle segments introduces a dynamic load.

The NASTRAN model of the turbine wheel and rotor (Fig. 2-4) was loaded with a centrifugal load simulating the operating speed and the constant pressure loads shown in Fig. 2-5. This loading resulted in a maximum outward radial deflection of .0022 in.

The natural frequencies of the turbine wheel and rotors were extracted and the mode shapes plotted as shown in Figs. 2-6 through 2-11. The Campbell diagram of Fig. 12 shows a potential resonance at the first mode-fourth harmonic. It was speculated that this excitation could occur due to the passing in and out of blocked nozzle passage regions. However, the application of this dynamic load produced results that did not indicate the presence of a resonance condition. Output plots of labyrinth seal displacement versus turbine wheel rotational position shown in Figs. 2-13 and 2-14 indicate that the output response basically tracks the input load without the large displacements characteristic of a resonance. This leads to the conclusion that for both the symmetric and the non-symmetric blockage pattern, the dynamic loading produces only a forced response. The maximum magnitude of the response at the labyrinth seal is .0004 in. for the symmetric blockage and .0032 in. for the non-symmetric.

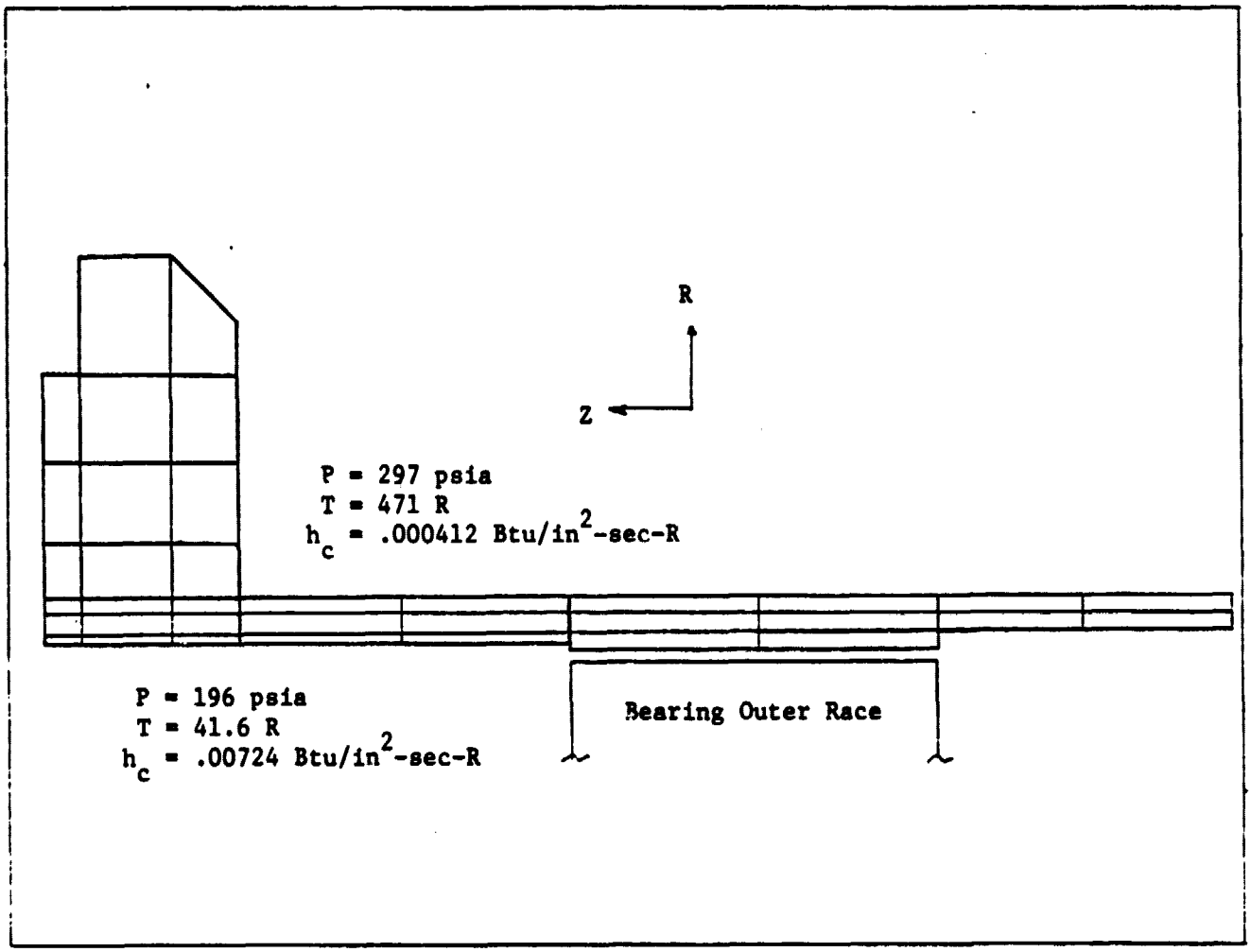

Fig. 2-2 LPFTP Bearing Carrier Environment

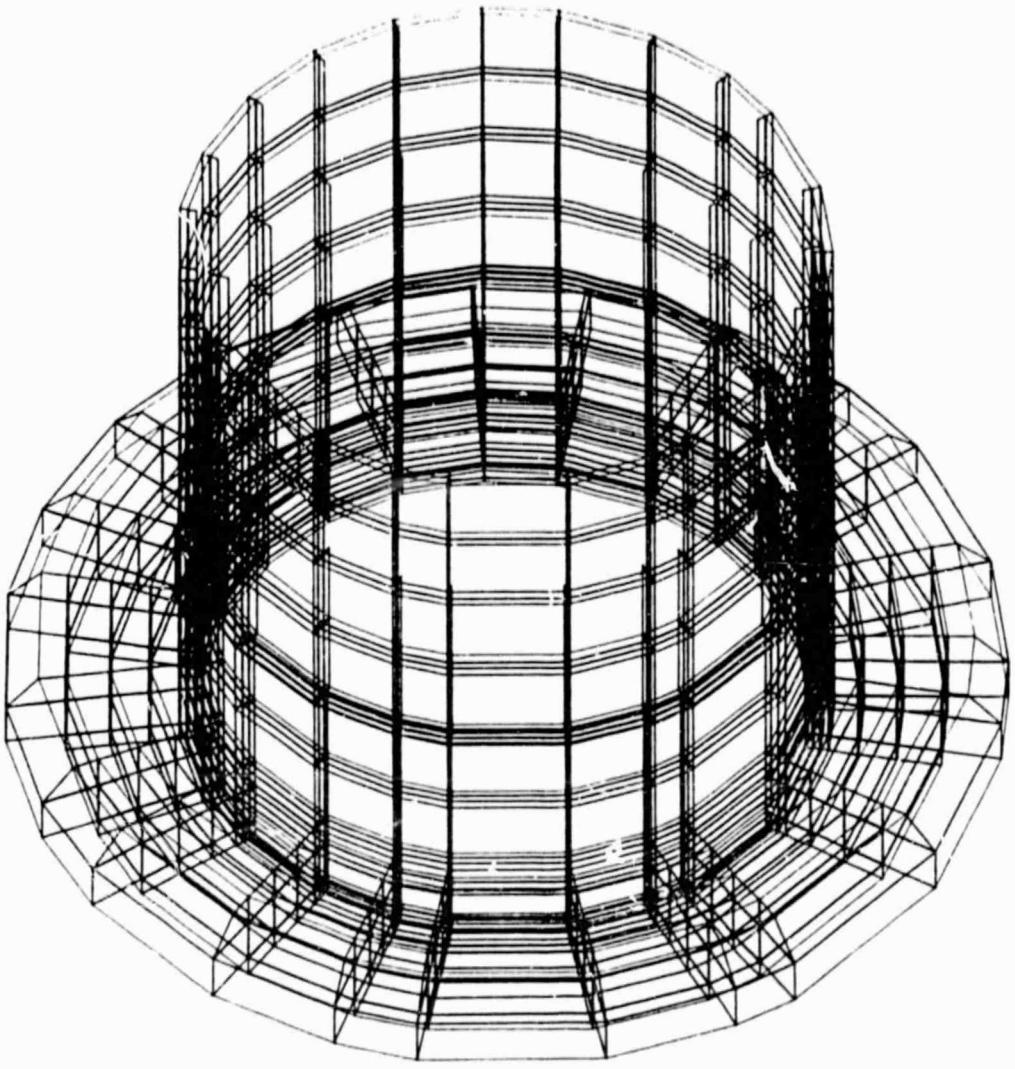

Fig. 2-3 NASTRAN LPFTP Bearing Carrier Model

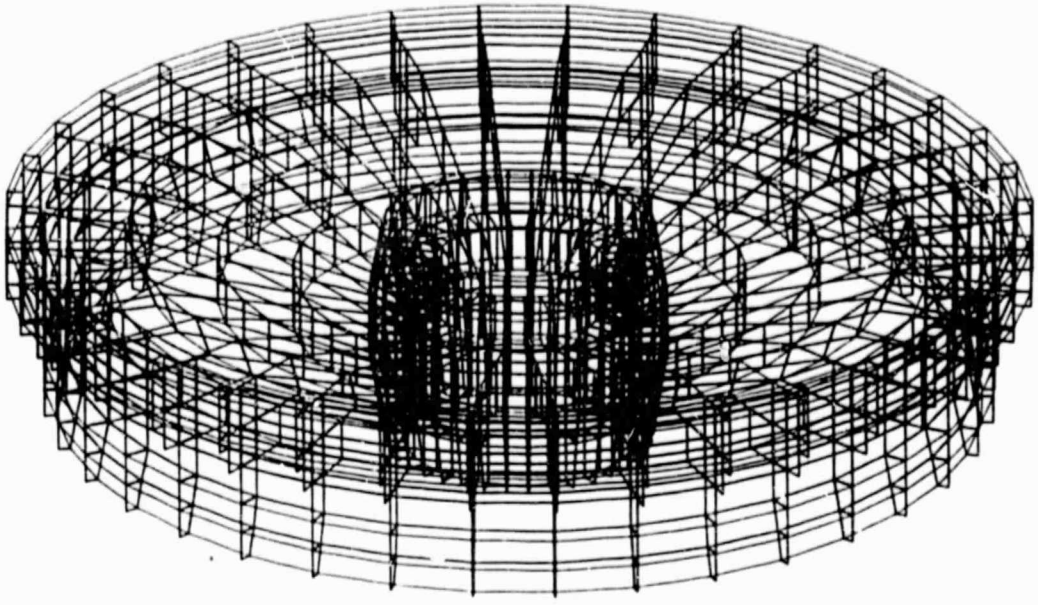

Fig. 2-4 LPFTP Turbine Wheel Model

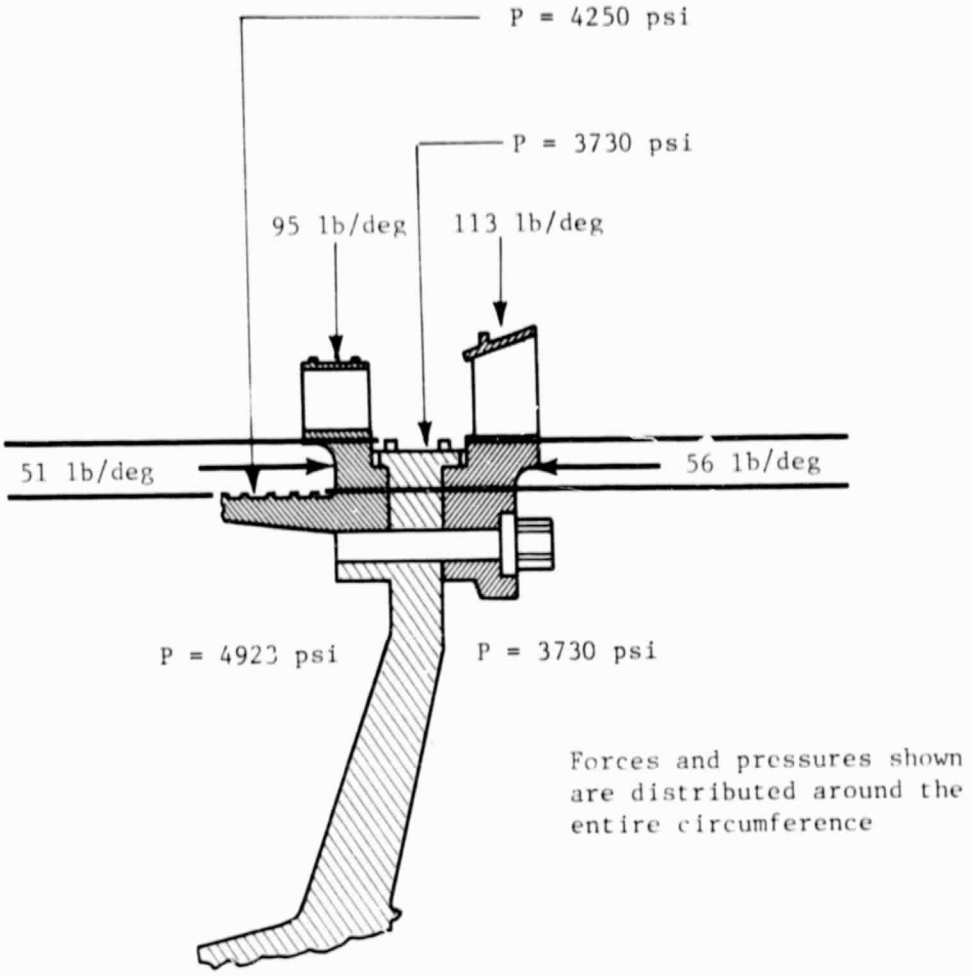

Fig. 2-5 LPFTP Turbine Wheel and Rotors (Static Loading)

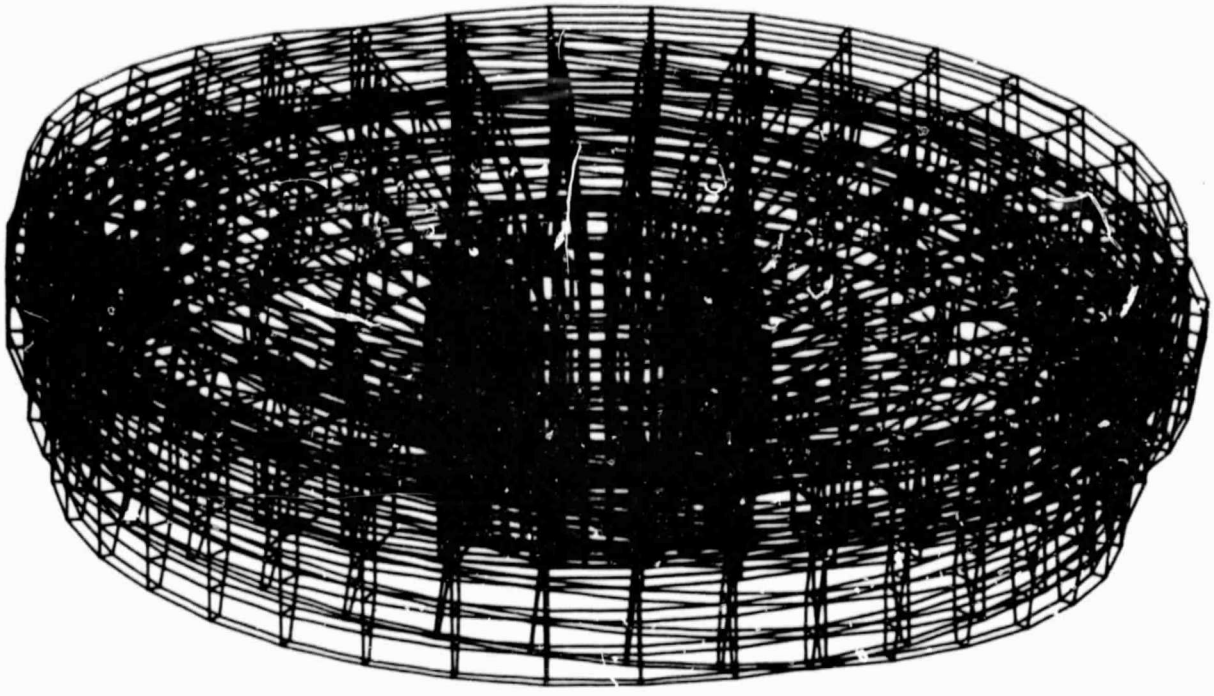

Fig. 2-6 LPFTP Turbine Disk, Mode 1, 1105 Hz

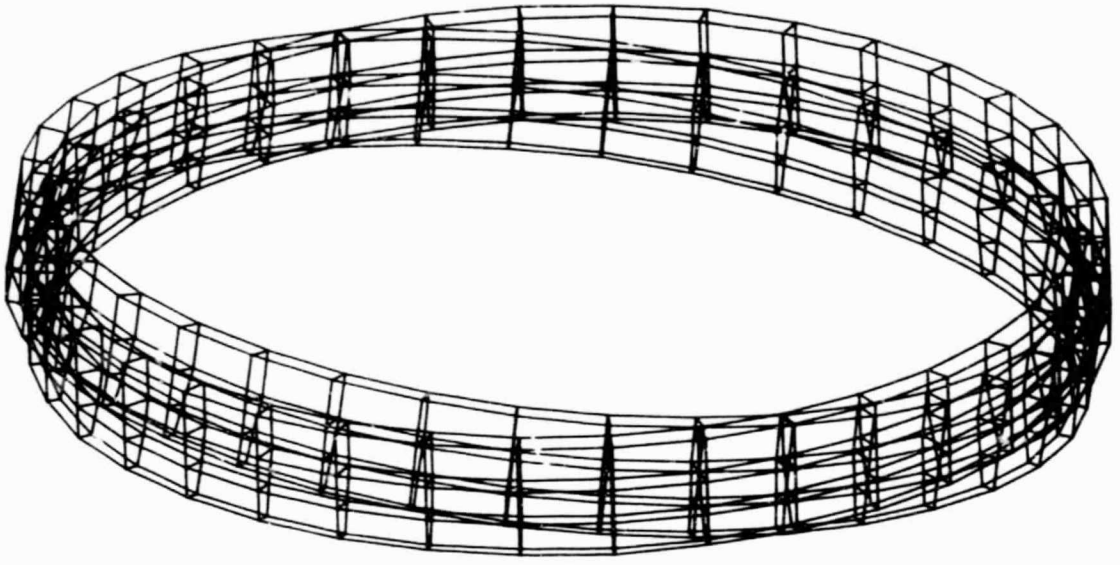

Fig. 2-7 LPFTP Turbine Labyrinth Seal, Mode 1, 1105 Hz

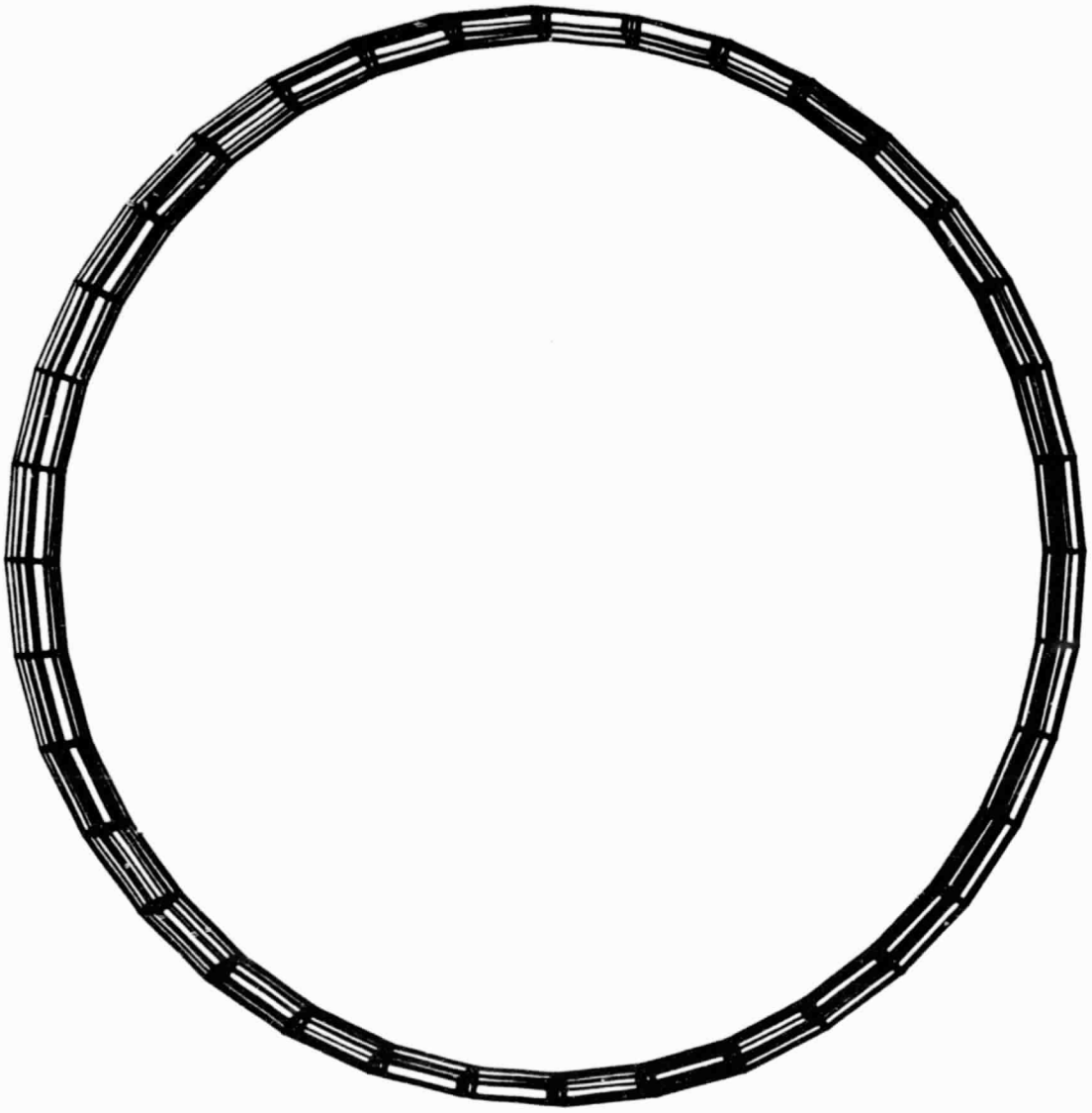

Fig. 2-8 LPFTP Turbine Labyrinth Seal, Mode 1, 1105 Hz

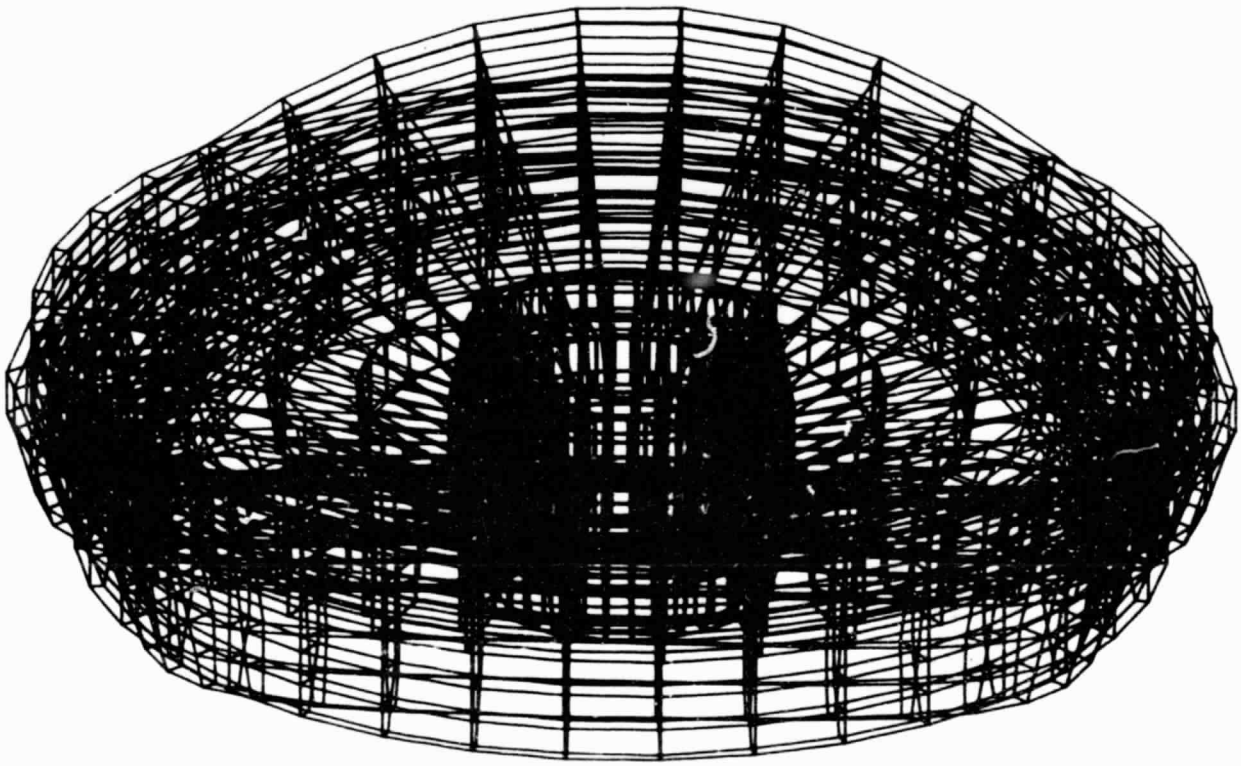

Fig. 2-9 LPFTP Turbine Disk, Mode 2, 1330 Hz

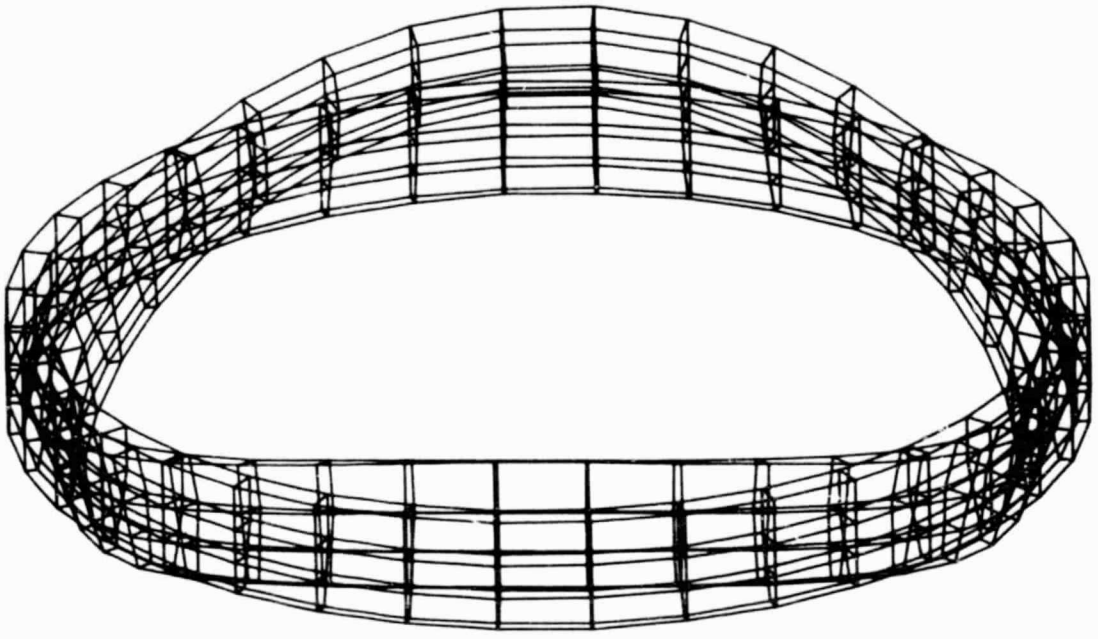

Fig. 2-10 LPFTP Turbine Labyrinth Seal, Mode 2, 1330 Hz

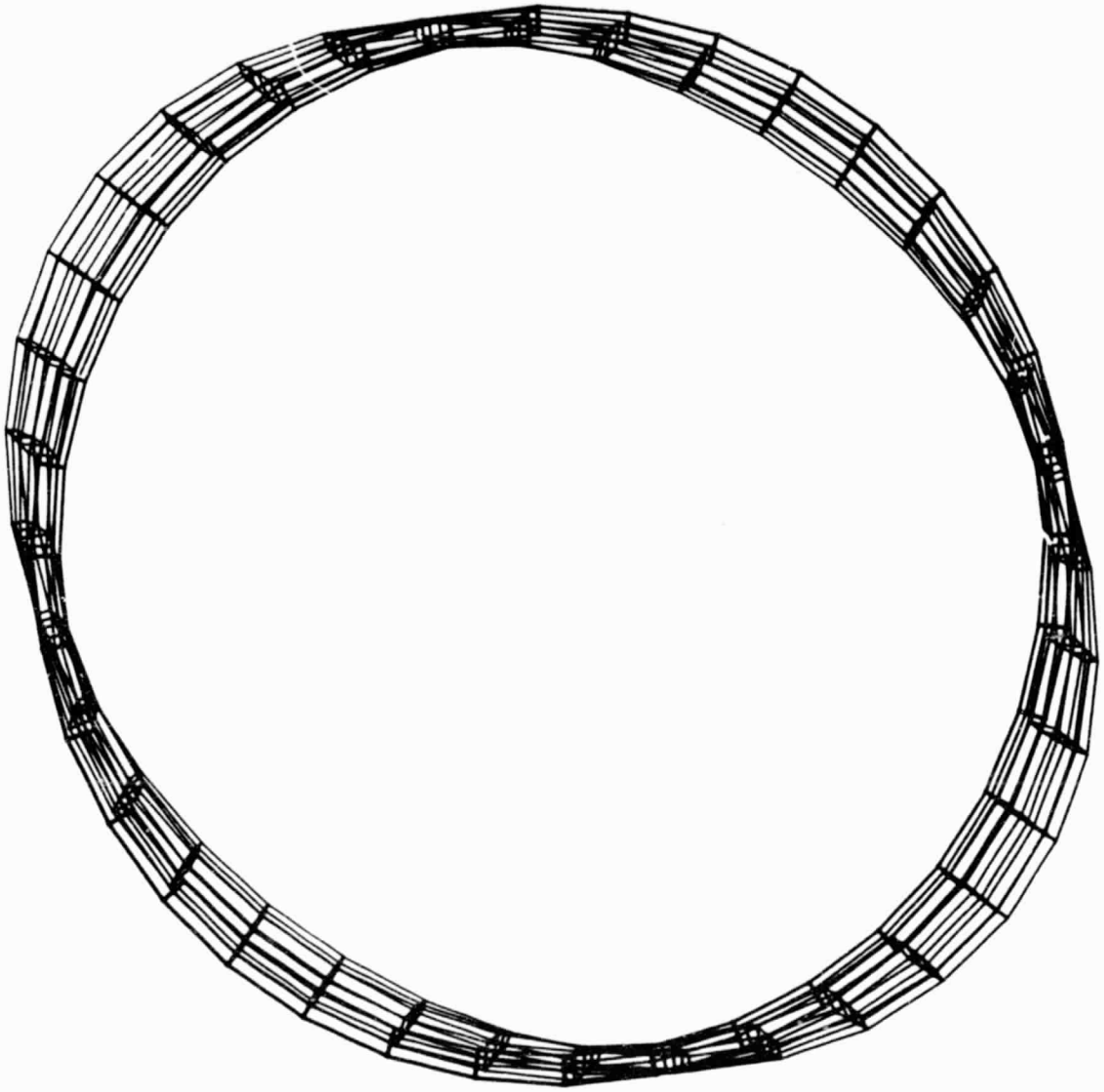

Fig. 2-11 LPFTP Turbine Labyrinth Seal, Mode 2, 1330 Hz

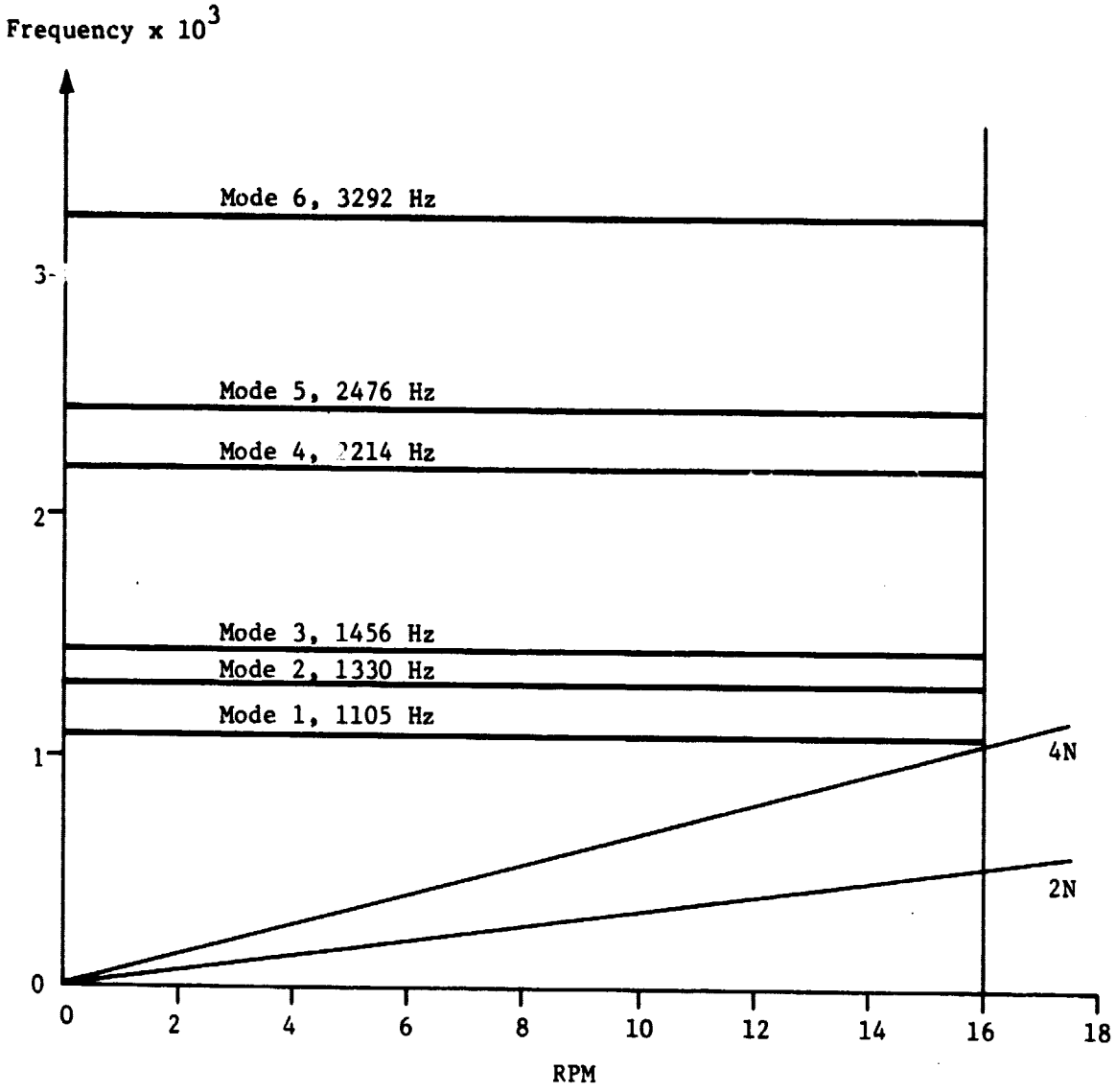

Fig. 2-12 LPFTP Turbine Disk - Campbell Diagram

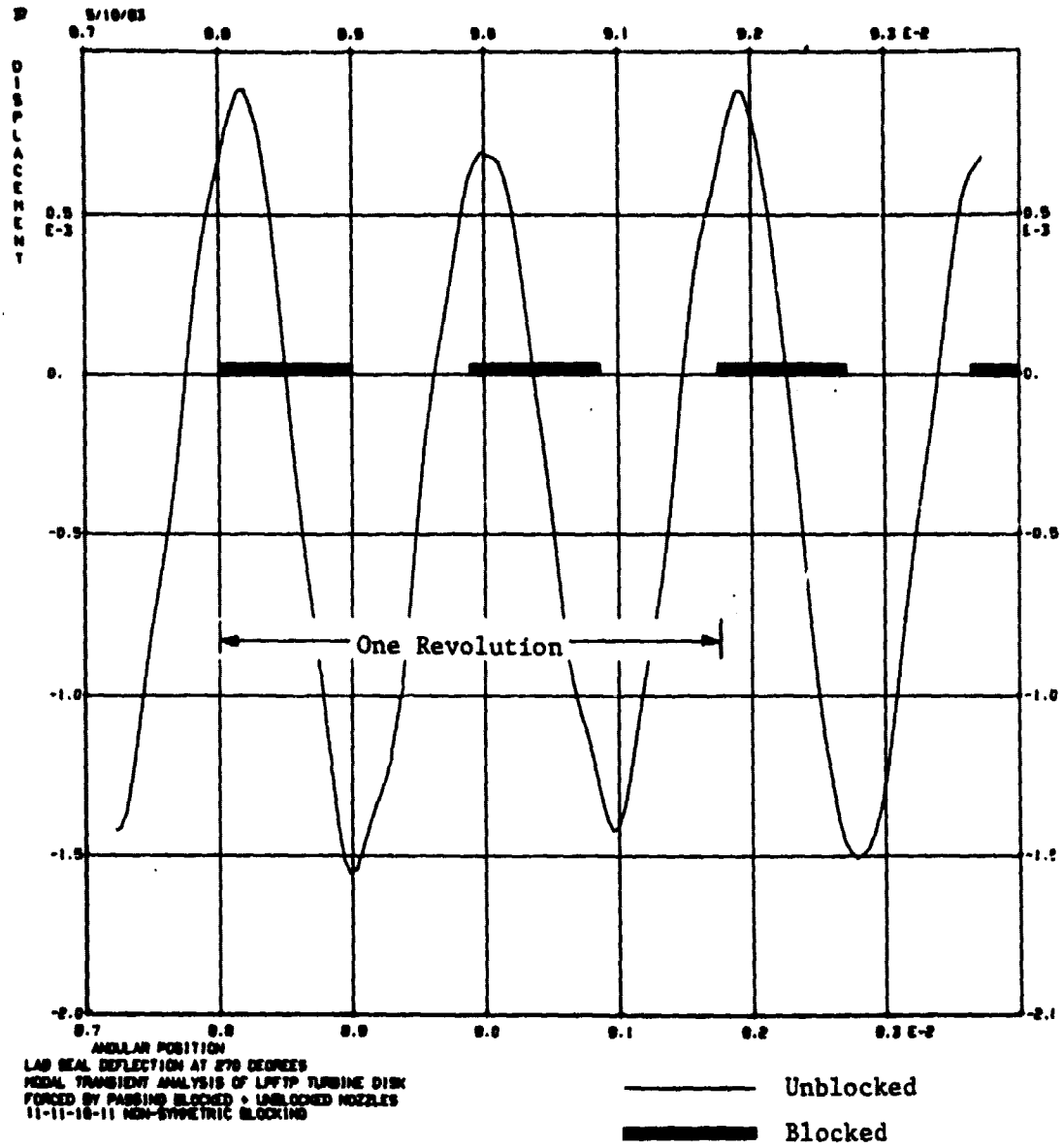

Fig. 2-13 Labyrinth Seal Deflection vs Rotation (Symmetric Blocking)

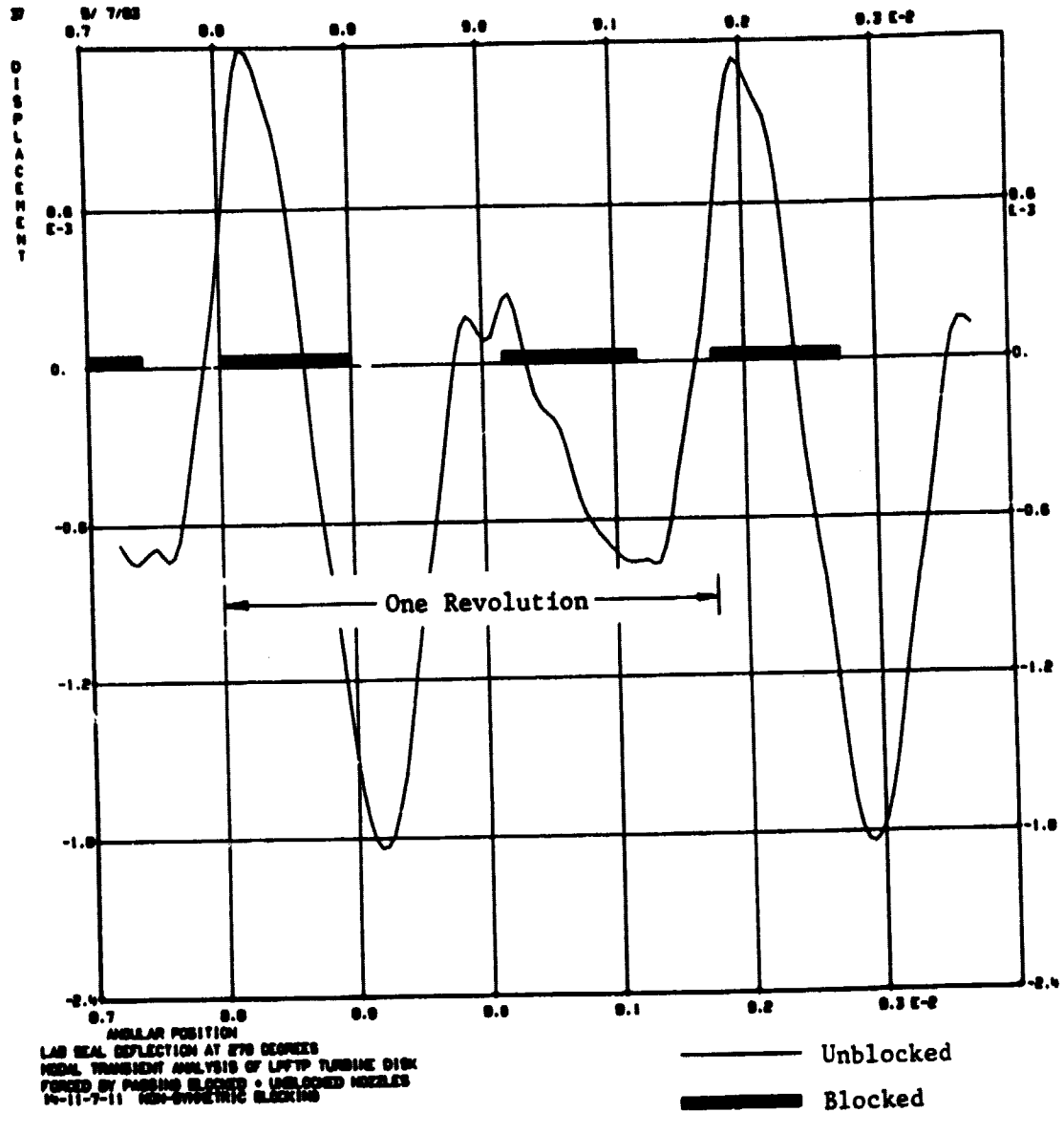

Fig. 2-14 Labyrinth Seal Deflection vs Rotation - Non-Symmetric Blocking

2.3 NOZZLE ASSEMBLY AND INLET MANIFOLD

The pressure distribution in the inlet manifold and pressure on the nozzle blockages act to produce radial deflections of the nozzle assembly directly opposite the labyrinth seal. The circumferential variation in the geometry of the inlet manifold volute and the nature of the pressure distribution in the volute tend to force the nozzle assembly into a non-circular shape and a potential rubbing configuration.

NASTRAN models of the inlet manifold (Fig. 2-15) and nozzle assembly (Fig. 2-16) were built and merged (Fig. 2-17) to show the effects of the inlet manifold pressure distribution on the surface opposite the labyrinth seal. The pressure distribution described in Figs. 2-18 and 2-19 was applied and produced the radial deflections at the labyrinth seal area shown in Fig. 2-20. The deflections are inward (closing the labyrinth seal gap) and range from a minimum of .0001 in. to a maximum of .0015 in.

2.4 SUMMARY OF LPFTP LABYRINTH SEAL DEFLECTIONS

Deflections of the LPFTP labyrinth seal, as determined by computer analysis, are summarized below:

1. Bearing Carrier - Thermal and Pressure Loads

   Bearing Carrier - Outer Race Clearance: .0038 in

   Extrapolate Axially to Labyrinth Seal: .0058 in.

2. Turbine Disk - Pressure and Centrifugal Loads

   Labyrinth Seal Maximum Radial Deflection: .0022 in.

3. Turbine Disk - Forced by Blocked Passages

   a. Non-Symmetric Blockage
      Labyrinth Seal Maximum Radial Deflection: .0032 in.

   b. Symmetric Blockage
      Labyrinth Seal Maximum Radial Deflection: .0004 in.

4. Inlet Manifold and Nozzle Assembly-Pressure Loads

Sealing Surface Maximum Radial Deflection: .0015 in.

Assume Worst-on-Worst and Superposition

Total Radial Deflections:

a. Non-Symmetric Blockage: .0127 in.

b. Symmetric Blockage: .0099 in.

Allowable Labyrinth Seal Tolerance from Drawing Specifications:

Minimum: .009 in.
Maximum: .011 in.

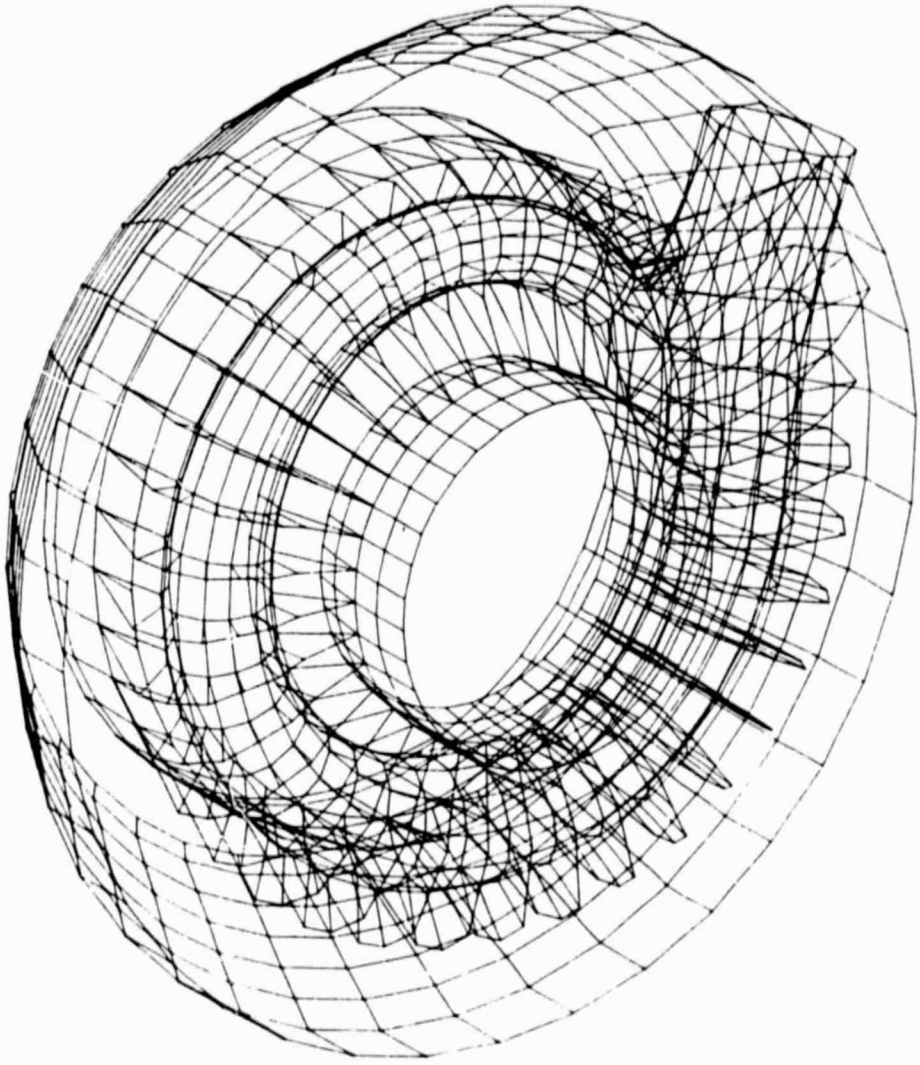

Fig. 2-15 LPFTP Inlet Manifold NASTRAN Model

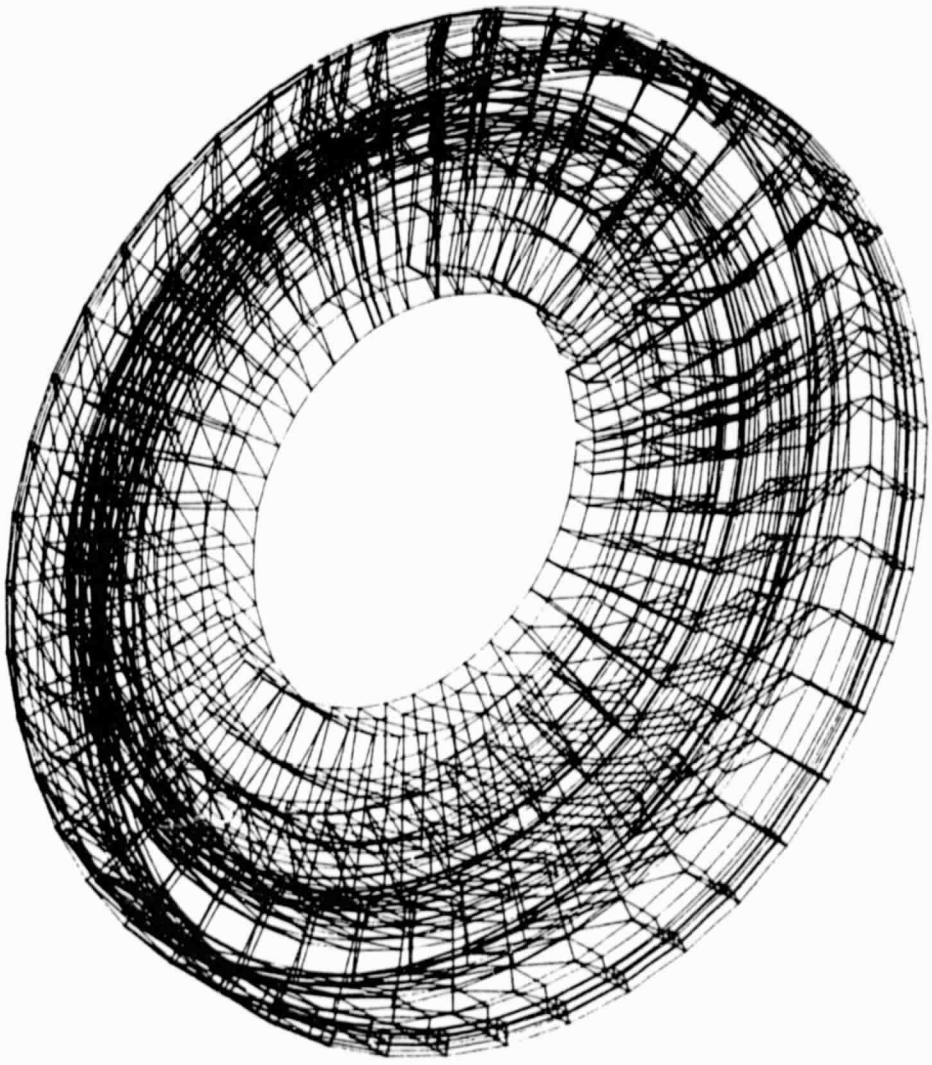

Fig. 2-16 LPFTP Turbine Inlet Nozzles - NASTRAN Model

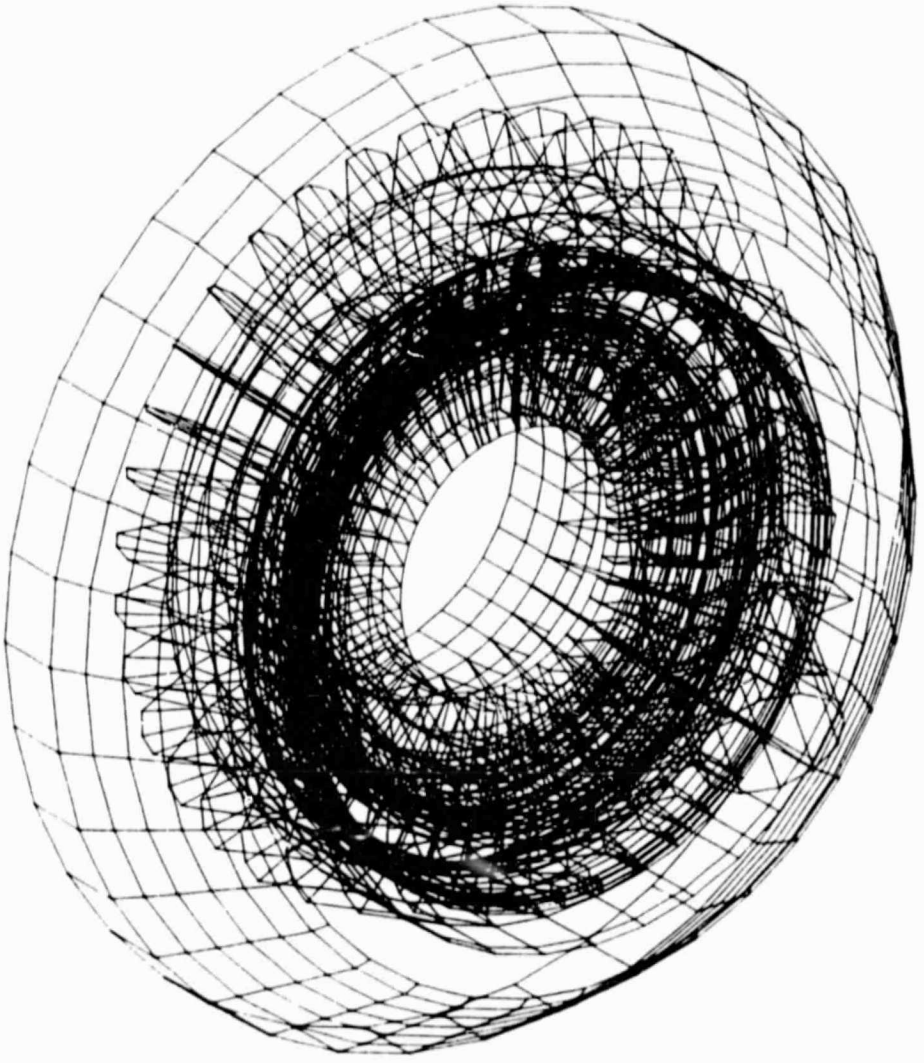

Fig. 2-17 LPFTP Inlet Manifold and Turbine Inlet Nozzles - Combined NASTRAN Model

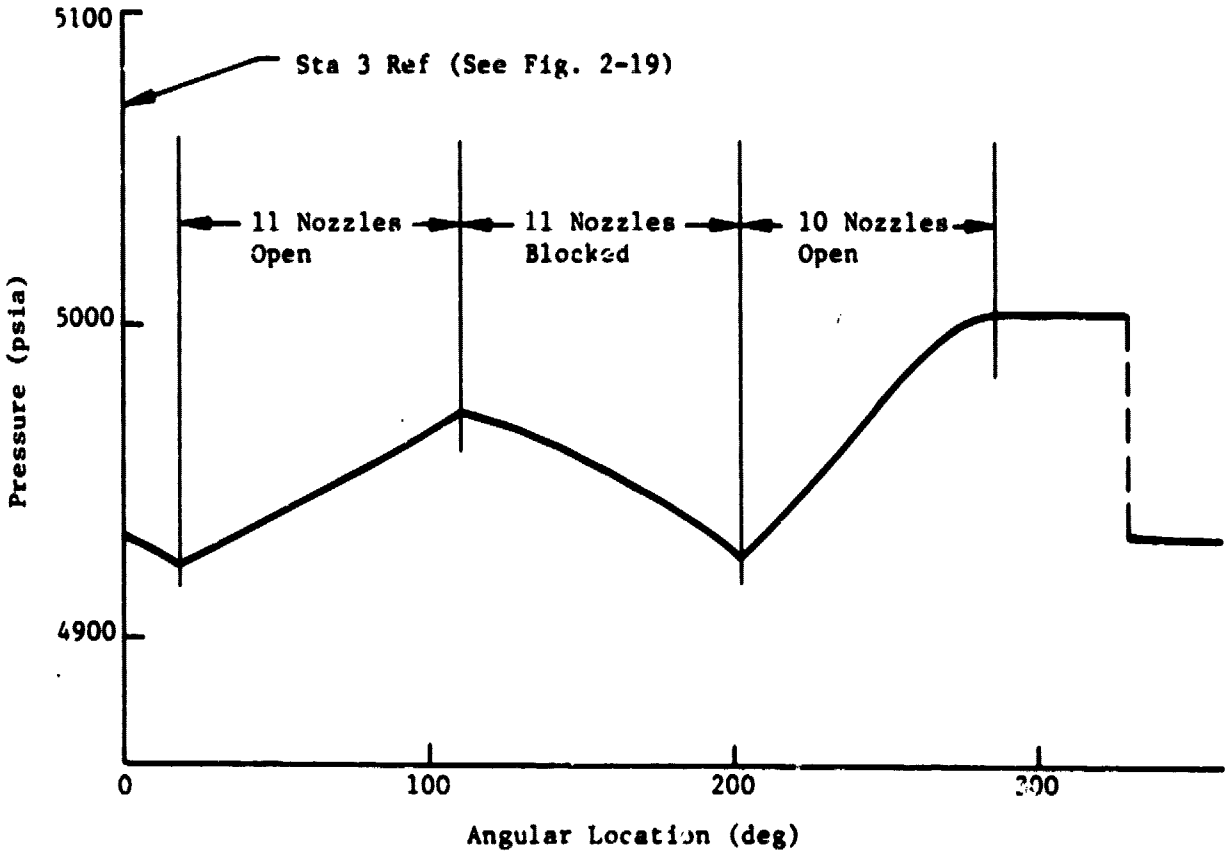

Fig. 2-18 LPFTP Turbine Inlet Manifold Pressure Distribution

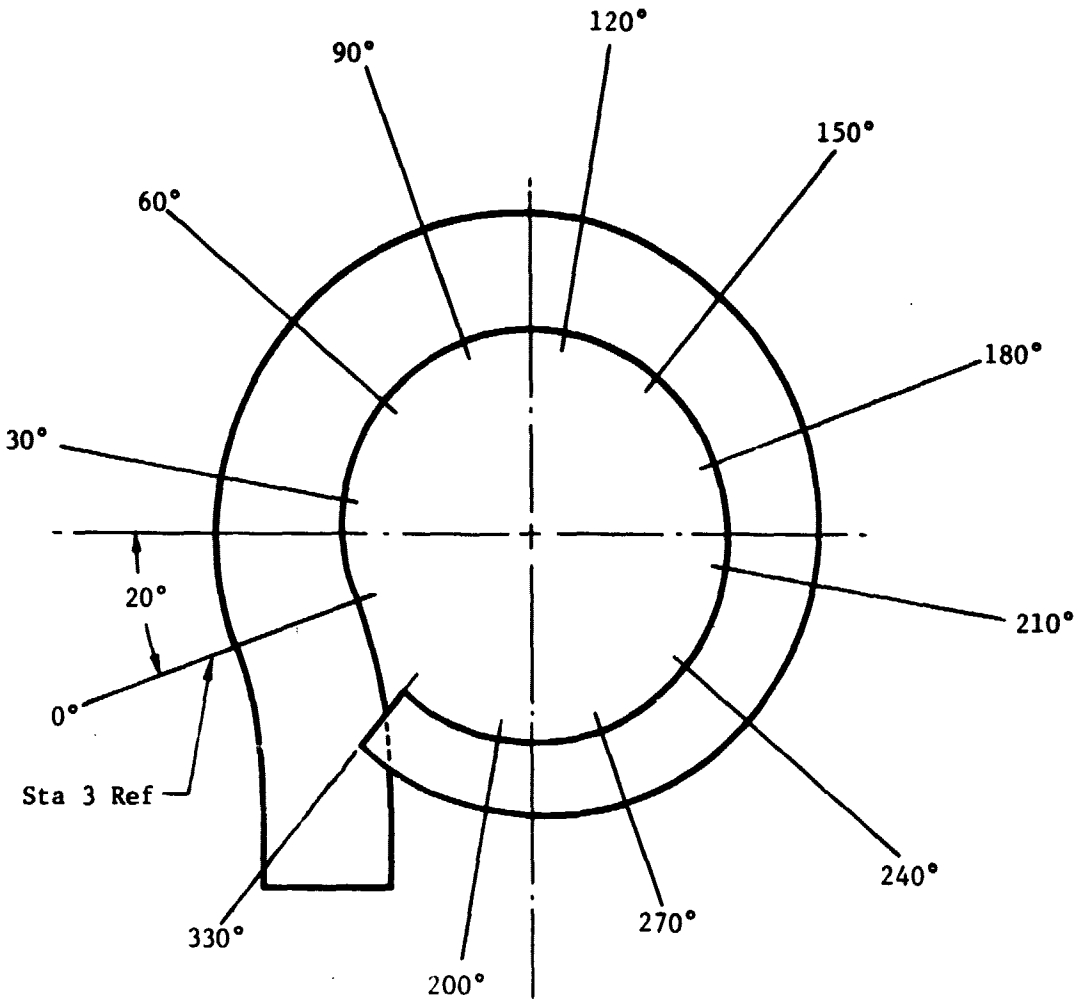

Fig. 2-19 LPFTP Turbine Inlet Manifold Angular Locations for Pressure Distribution (Fig. 2-18)

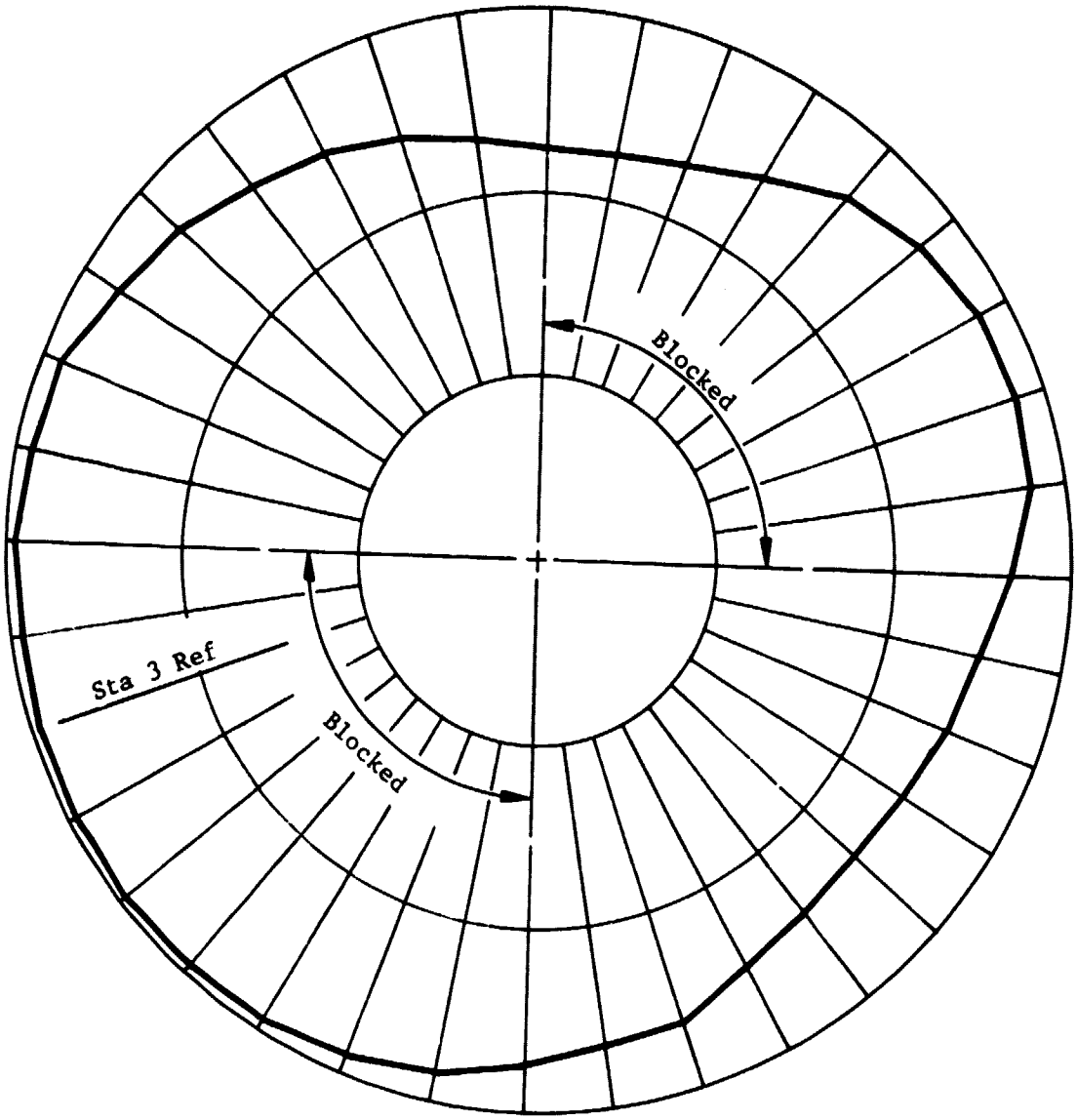

Fig. 2-20 LPFTP Turbine Inlet Nozzle Labyrinth Seal Interface Deflections (Deflections Exaggerated - Max = 1.5 x 10^{-3} in.)

3. GAS DYNAMICS ANALYSES

3.1 HPFTP SECOND STAGE TURBINE DISK COOLANT MODIFICATION ANALYSIS

The HPFTP second stage turbine blades have experienced cracking in the aft shank region near the platform. One possible cause for these cracks is high thermal gradients resulting from the cold hydrogen coolant which flows up the back side of the disk. A modification to route the hydrogen coolant through six slots near the I.D. of the aft platform seal has been proposed. The HPFTP turbine coolant system flow model (Ref. 3.1) was modified to simulate this configuration. The model is shown schematically in Fig. 3-1. Flow rates and temperatures at several points of interest are compared with the nominal FPL case in Table 3-1.

3.2 HPFTP TURBINE HOUSING HOT GAS LEAKAGE ANALYSIS (EFFECT ON COOLANT LINER PRESSURE

The HPFTP turbine coolant model was modified to simulate leakage of turbine gases into the coolant system downstream of the coolant liner. The leakage path is assumed to be cracks in the turbine housing downstream of the second stage rotor. The turbine coolant system (with the modification included) is shown in Fig. 3-2. Coolant liner pressure and leakage flow rate versus leakage area are shown in Fig. 3-3.

3.3 HPFTP IMPELLER SHAFT AND SHROUD SEALS MODIFICATIONS

3.3.1 Leakage Analysis with Nominal Operating Clearances

The HPFTP impeller flow models (Ref. 3.1) were updated to simulate the redesigned shaft and shroud seals. Designating the previous configuration

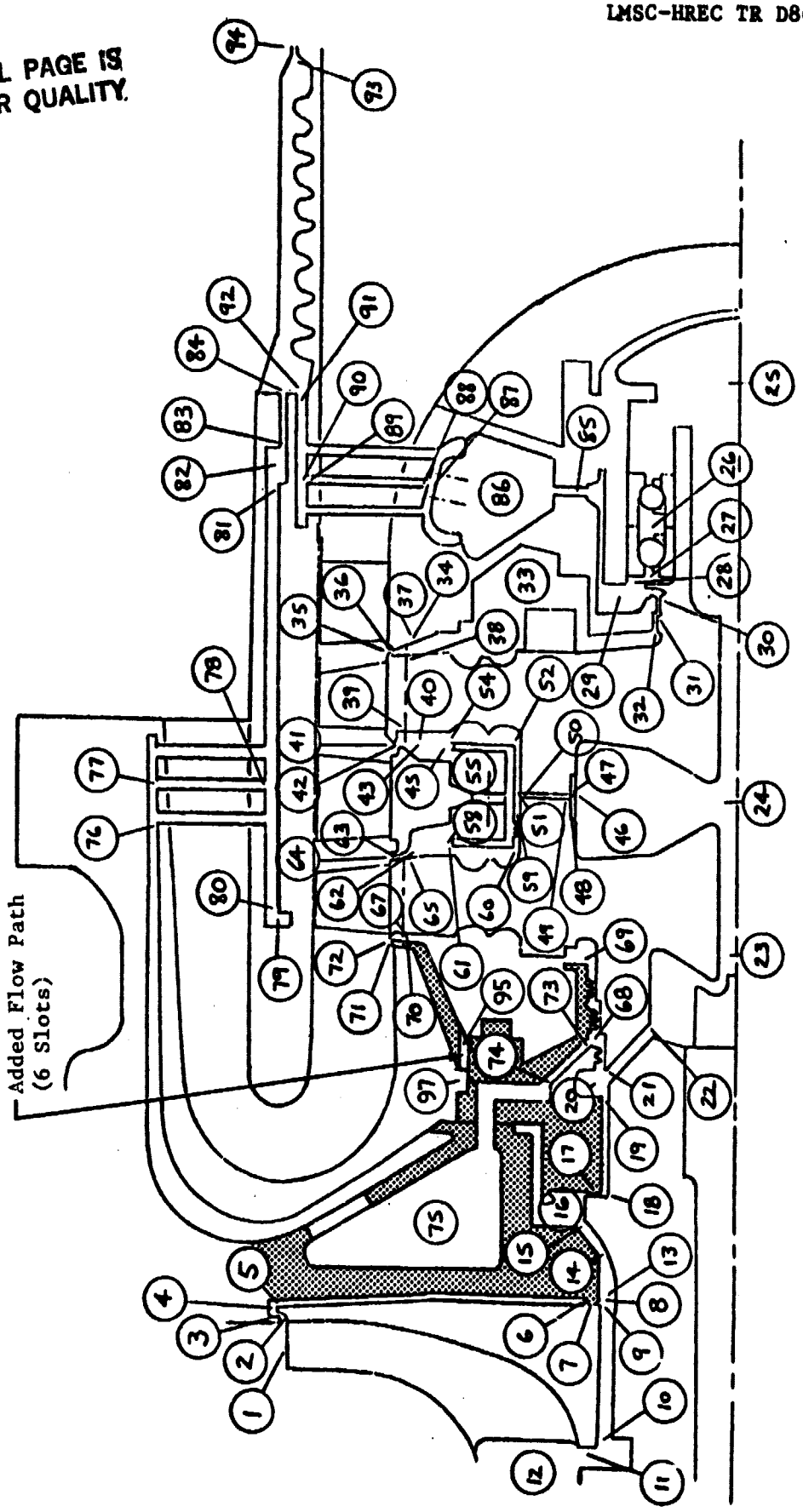

Fig. 3-1 HPFTP Turbine Coolant System Schematic with Second Stage Disk Coolant Modification

Table 3-1 HPFTP SECOND STAGE TURBINE DISK COOLANT MODIFICATION ANALYSIS
(Slot Area = .342 in^2)

	Nominal Configuration		Modified Configuration	
Station No.	Temperature (R)	Flow Rate (lbm/sec)	Temperature (R)	Flow Rate (lbm/sec)
16	141.7	2.583	141.7	2.818
23	145.1	1.721	145.2	1.898
29	145.8	0.957	146.0	1.069
33	146.8	0.516	147.5	0.642
35	1914.5	3.922	1914.5	4.365
41	1890.9	2.151	1890.9	2.854
51	155.4	0.764	156.1	0.830
64	1440.7	3.692	1450.3	2.734
66	1438.7	3.660	1448.7	5.956
69	145.3	0.360	146.1	0.458
72	1265.5	4.020	1468.0	3.308
76	174.8	0.502	177.1	0.462
95	—	—	1142.3	3.107

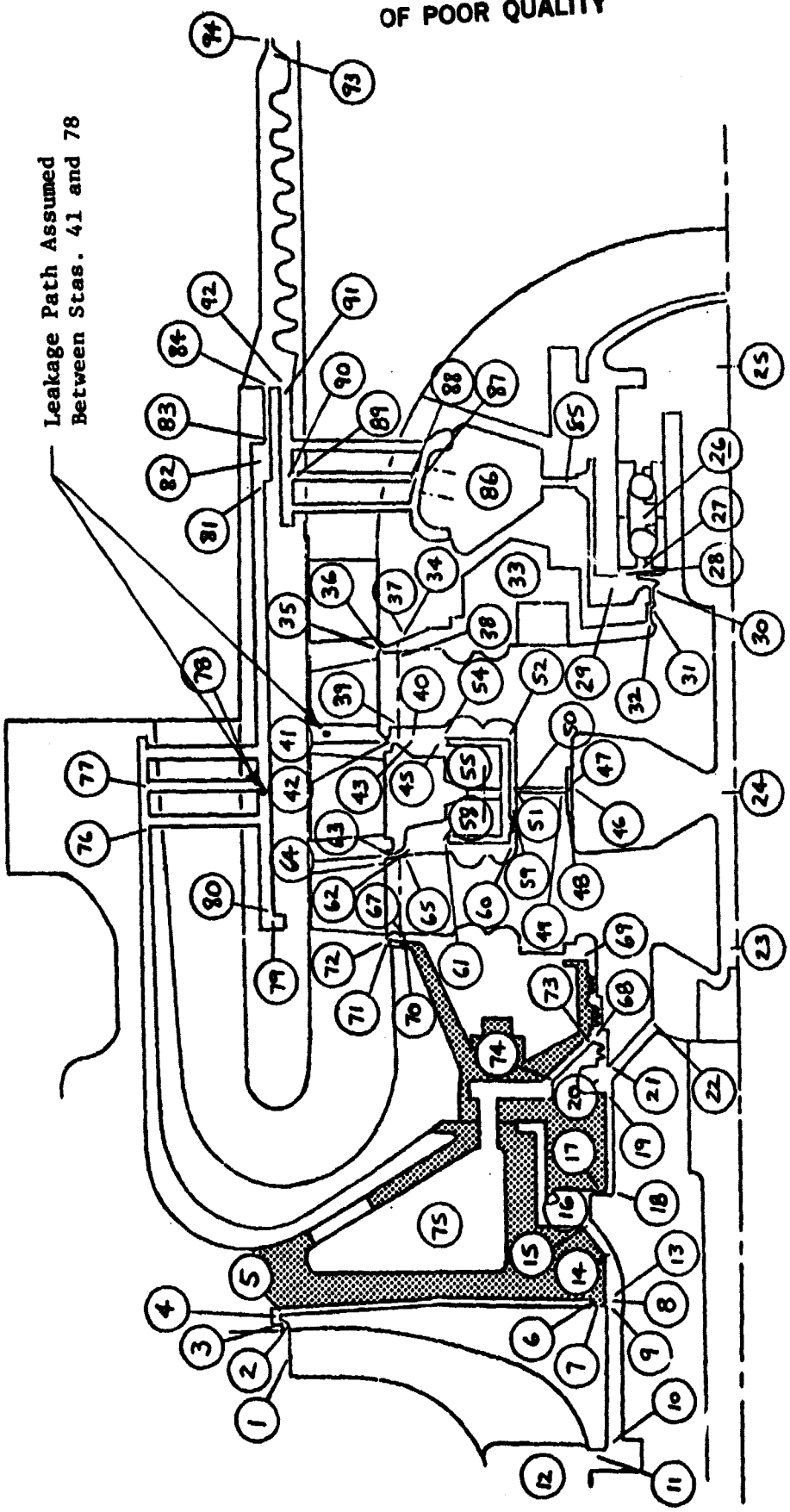

Fig. 3-2 HPFTP Turbine Coolant System Schematic with Turbine Housing Leakage Modification

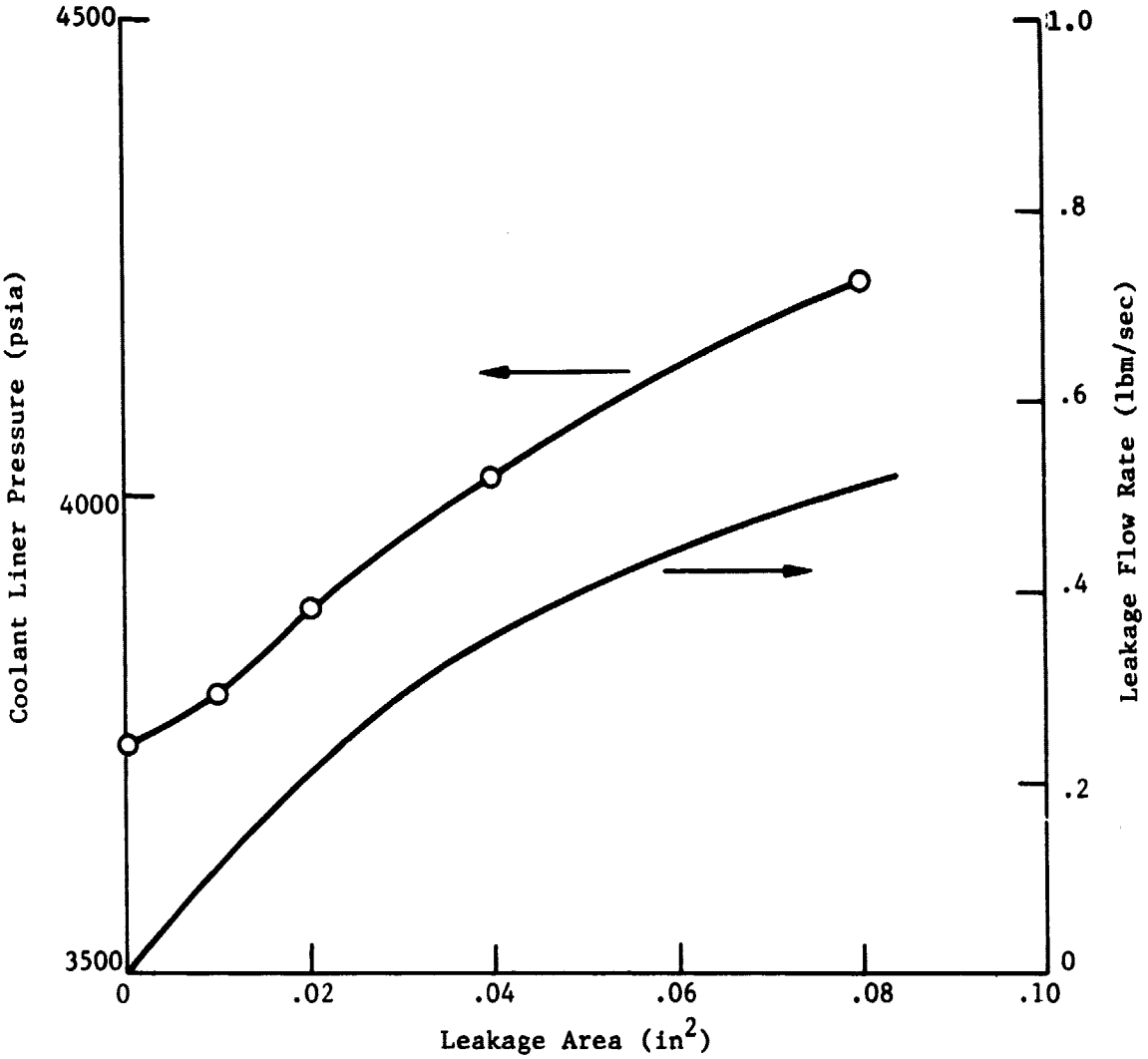

Fig. 3-3 HPFTP Turbine Housing Hot Gas Leakage Analysis

as "baseline" and the new configuration as "modified," a description of each configuration by part number is shown in Table 3-2.

Table 3-2 HPFTP IMPELLER SHAFT AND SHROUD SEAL CONFIGURATIONS

Stages	Baseline	Modified
First Stage		
Shaft Seal	RS007531-031	RS007531-041
Shroud Seal	RS007550-007	R0012199-3
Second Stage		
Shaft Seal	RS007531-031	RS007531-041
Shroud Seal	RS007530-007	R0012205-3
Third Stage		
Shroud Seal	RS007530-007	R0012205-3

Operating clearances for the modified configuration are shown in Figs. 3-4 and 3-5. Leakage flow rates are compared to the baseline configuration in Table 3-3.

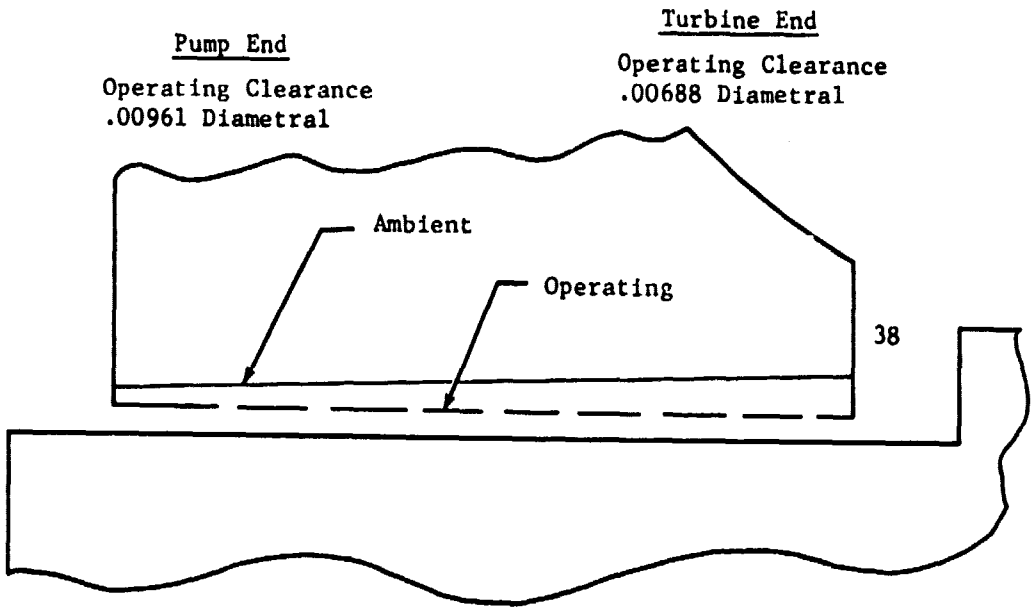

Fig. 3-4 HPFTP First and Second Stage Modified Shaft Seal Flow Schematic

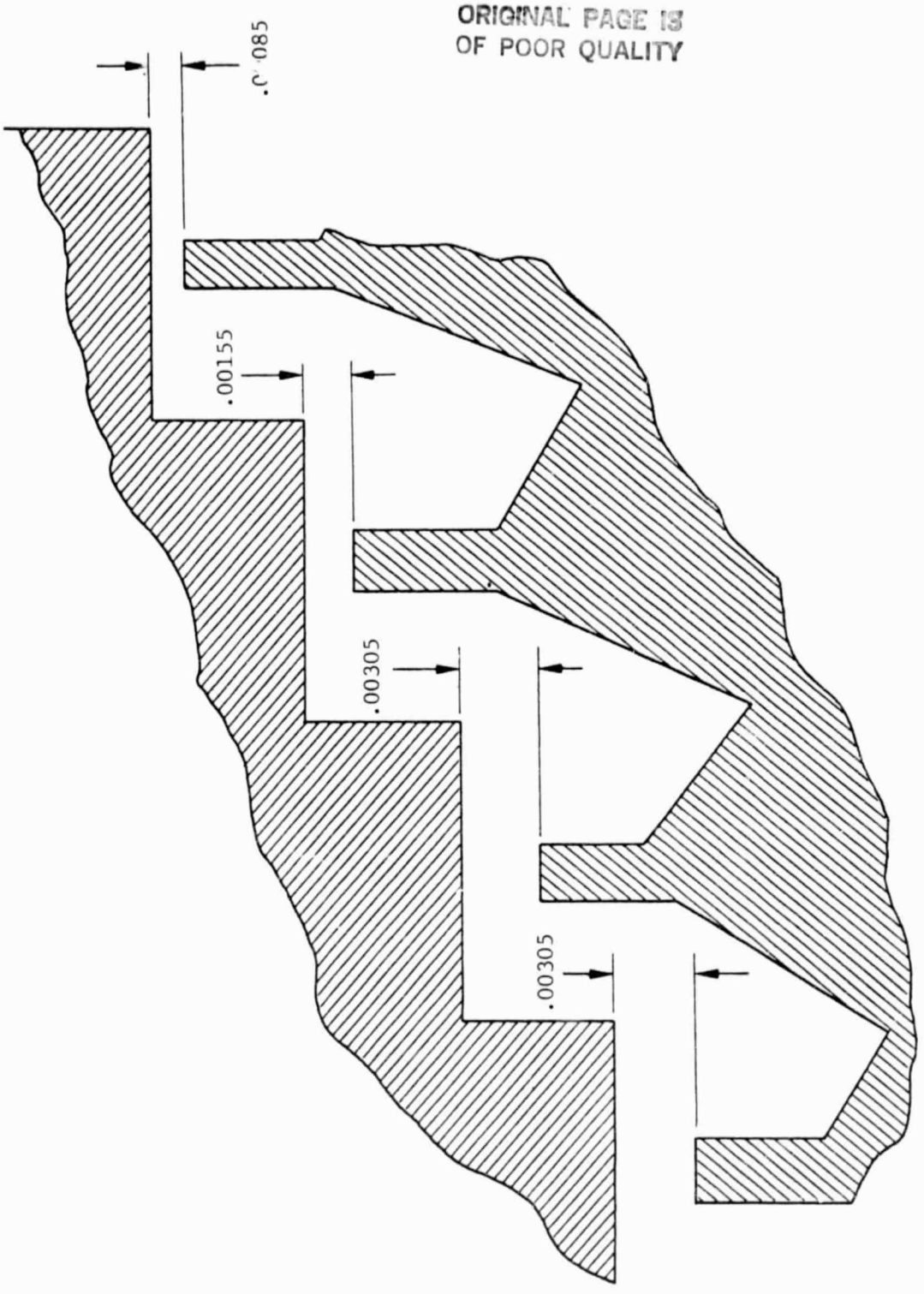

Fig. 3-5 HPFTP Modified Shroud Seal Operating Clearances

Table 3-3 HPFTP IMPELLER SHAFT AND SHROUD SEALS LEAKAGE COMPARISON

Stage	Baseline Flow Rate (lbm/sec)	Modified Flow Rate (lbm/sec)
First Stage		
Shaft Seal	1.41	1.14
Shroud Seal	2.75	0.37
Second Stage		
Shaft Seal	1.71	1.35
Shroud Seal	6.36	0.59
Third Stage		
Shroud Seal	5.39	0.67

3.3.2 Leakage Analysis with Axial Mismatch at the Shroud Seal

The HPFTP second stage impeller flow model was updated to accept a variable axial mismatch (using the first tooth as a reference point) between the teeth on the impeller shroud and the corresponding seal surface. The configuration is shown in Fig. 3-6 for an axial mismatch of .010 in. at the first tooth. Leakage flow rate versus first tooth axial mismatch is shown in Fig. 3-7.

3.4 HPOTP TURBINE BEARING COOLANT FLOW ANALYSIS

The HPOTP turbine bearing coolant model (Ref. 3.1) was used to analyze the coolant quality in the bearing cavity for the maximum variations which occur in inducer inlet pressure at power levels ranging from RPL to 111 percent. The input pressure data were supplied by NASA-MSFC and are shown in Fig. 3-8. The resulting bearing cavity temperature and pressure data are presented in Fig. 3-9 along with the saturation curve.

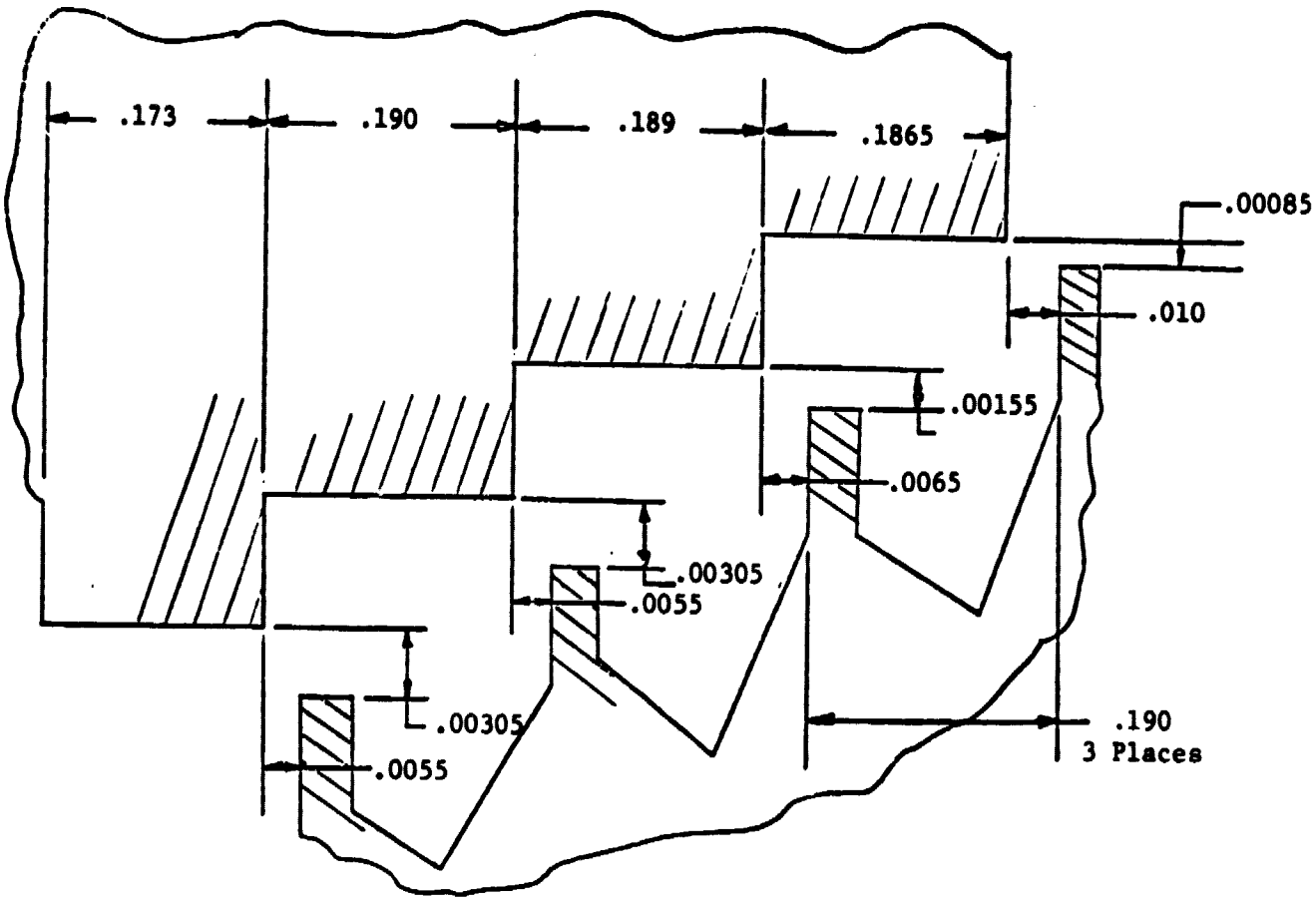

Fig. 3-6 HPFTP Modified Shroud Seal Clearances (First Tooth Axial Mismatch = .010)

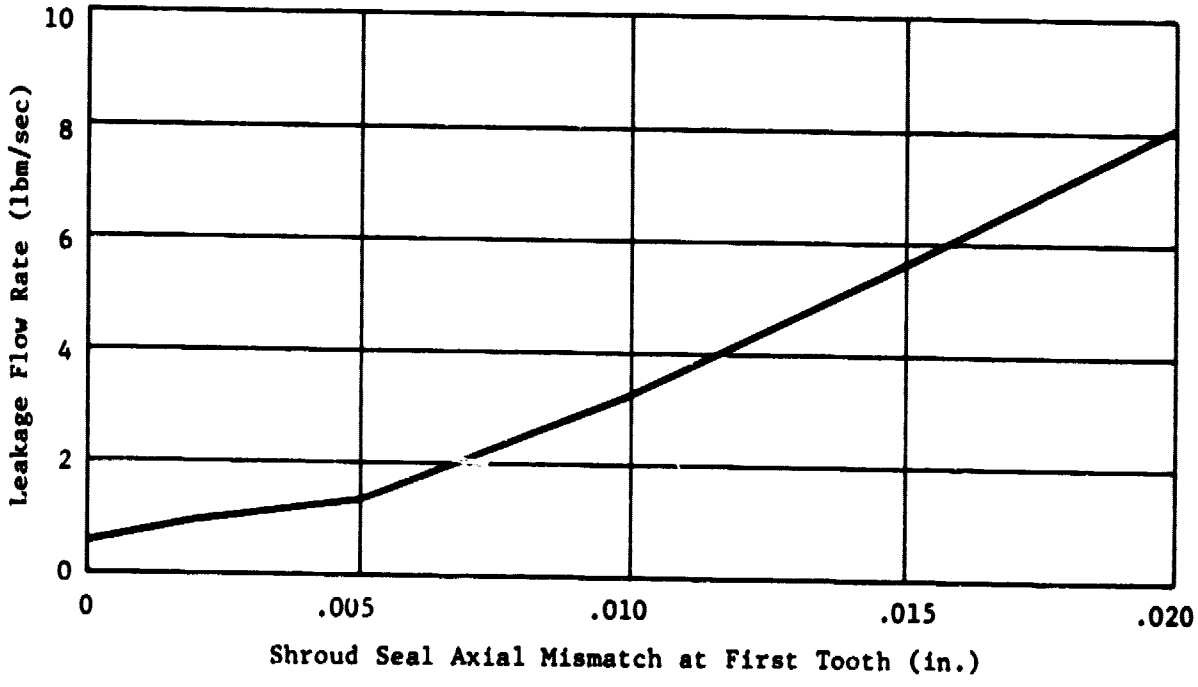

Fig. 3-7 HPFTP Second Stage Impeller Shroud Seal Leakage Analysis

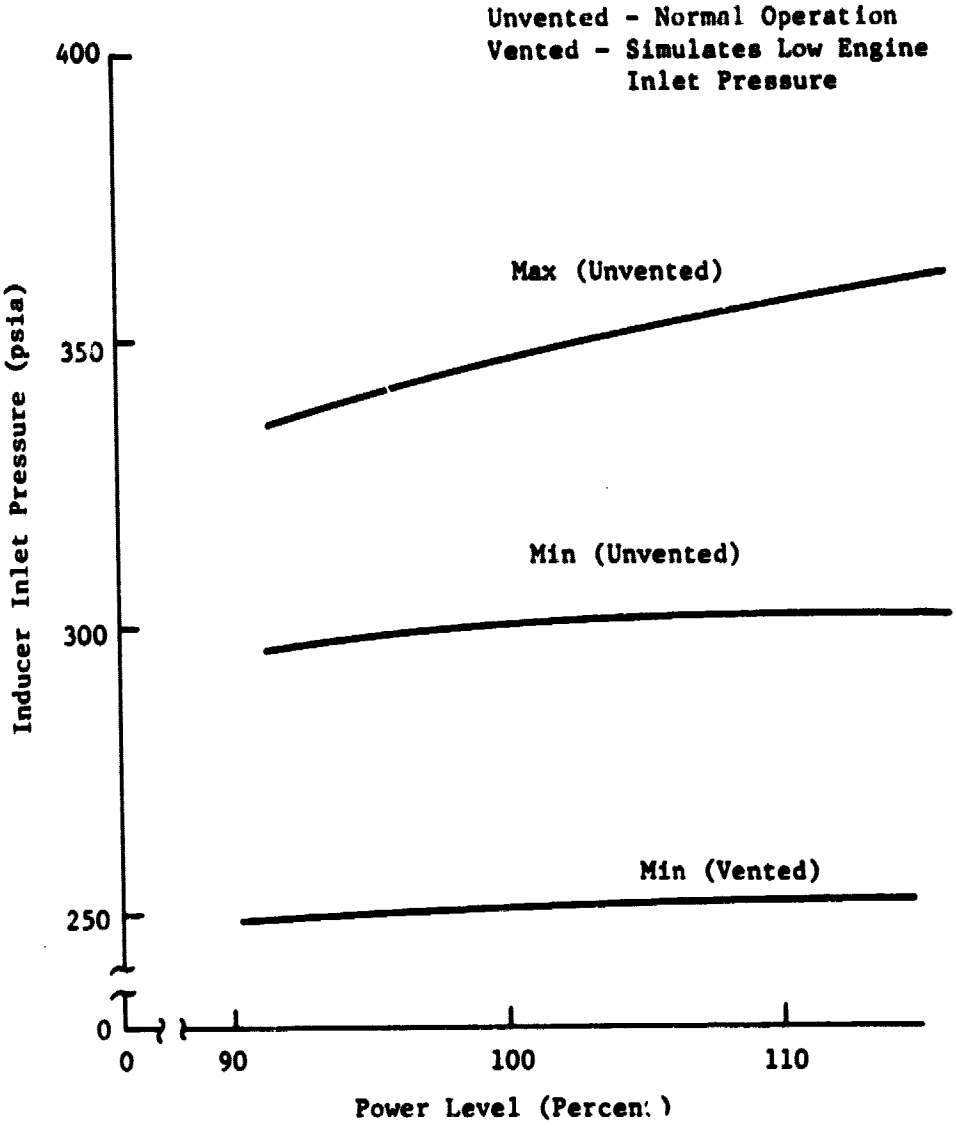

Fig. 3-8 HPOTP Inducer Inlet Pressure Range

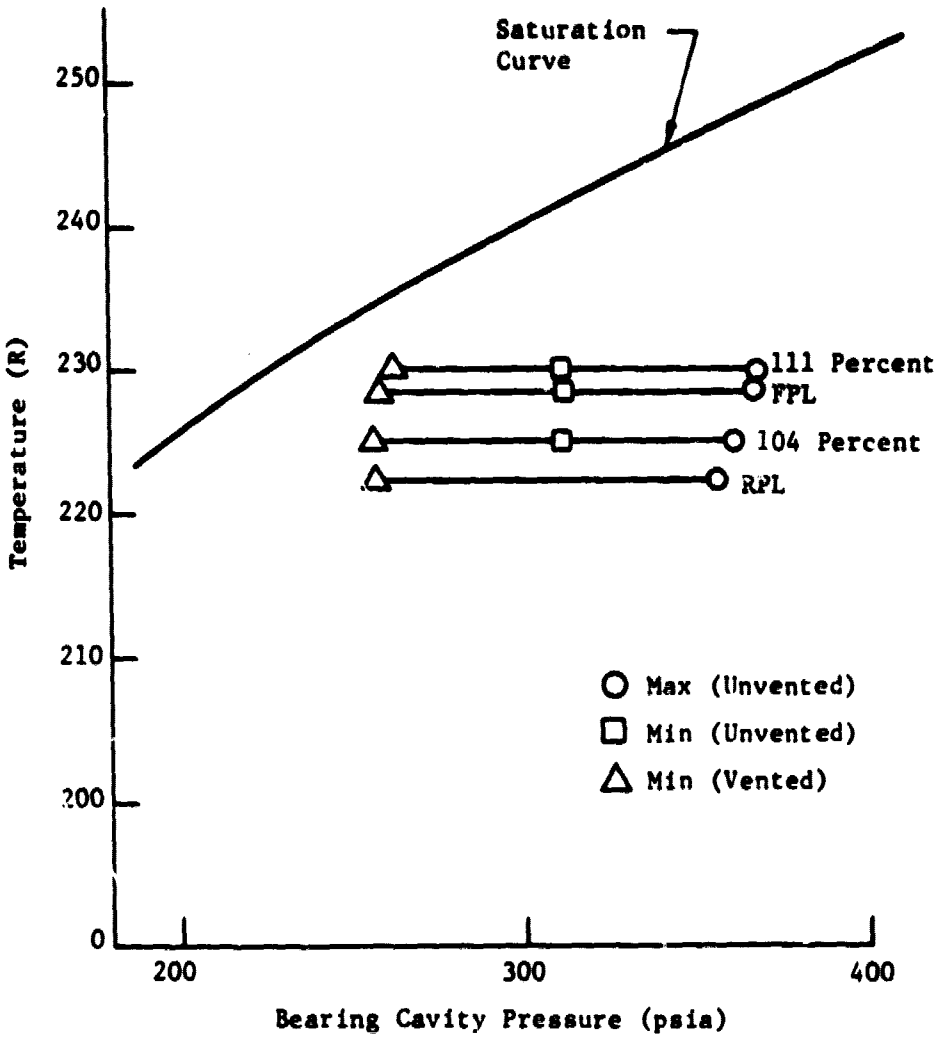

Fig. 3-9 HPOTP Turbine Bearing Coolant (Margin of Subcooling)

3.5 HPOTP PRIMARY OXIDIZER SEAL DRAIN ANALYSIS

3.5.1 Oxidizer Drain Analysis with Kel F Seal Removed

The turbine bearing coolant model was modified to simulate removal of the Kel F in the labyrinth seal and adding a simulation of the drain resistance. The model was then executed at RPL, 104 percent, FPL and 111 percent to determine drain cavity pressure and seal flow rate. The results are shown in Fig. 3-10.

3.5.2 Oxidizer Seal Analysis with Liquid Oxygen Leakage Through the Bearing Support Bolt Holes

The drain resistance was coupled with the bearing coolant model and a leakage path through the bearing support bolt holes. The model was executed with several leakage rates to determine the effect on drain cavity pressure. The results are presented in Fig. 3-11.

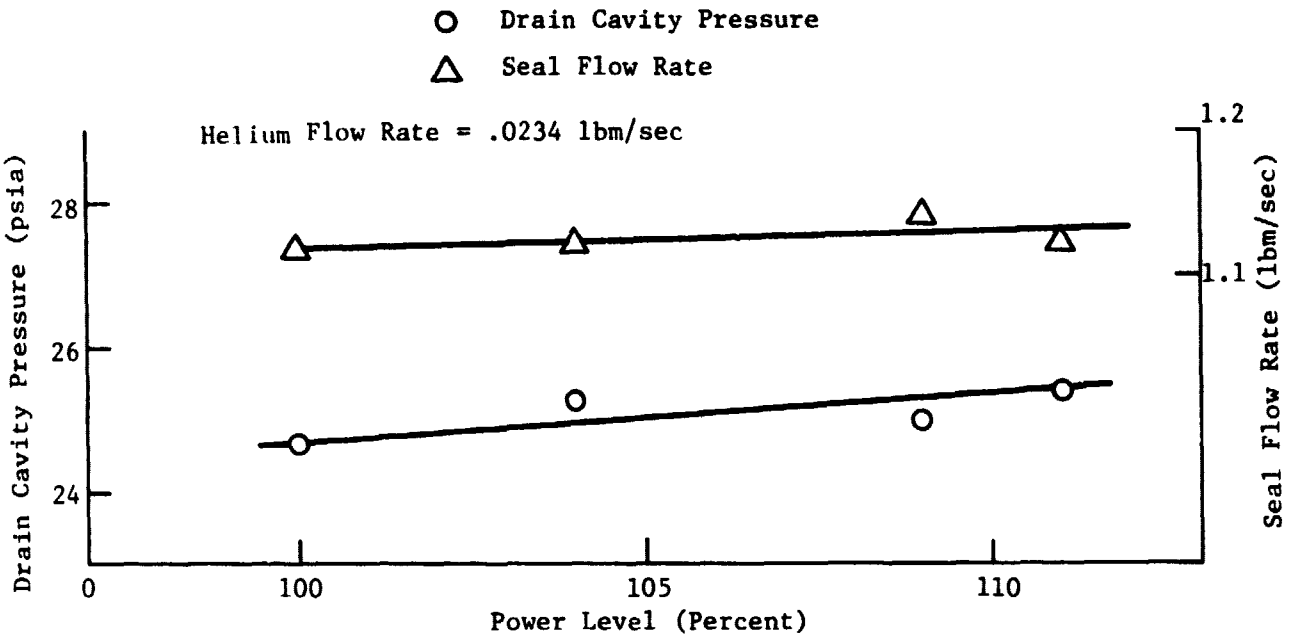

Fig. 3-10 HPOTP Turbine Bearing Coolant Model Coupled with Oxidizer Drain Resistance (Kel F Removed from Labyrinth Seal)

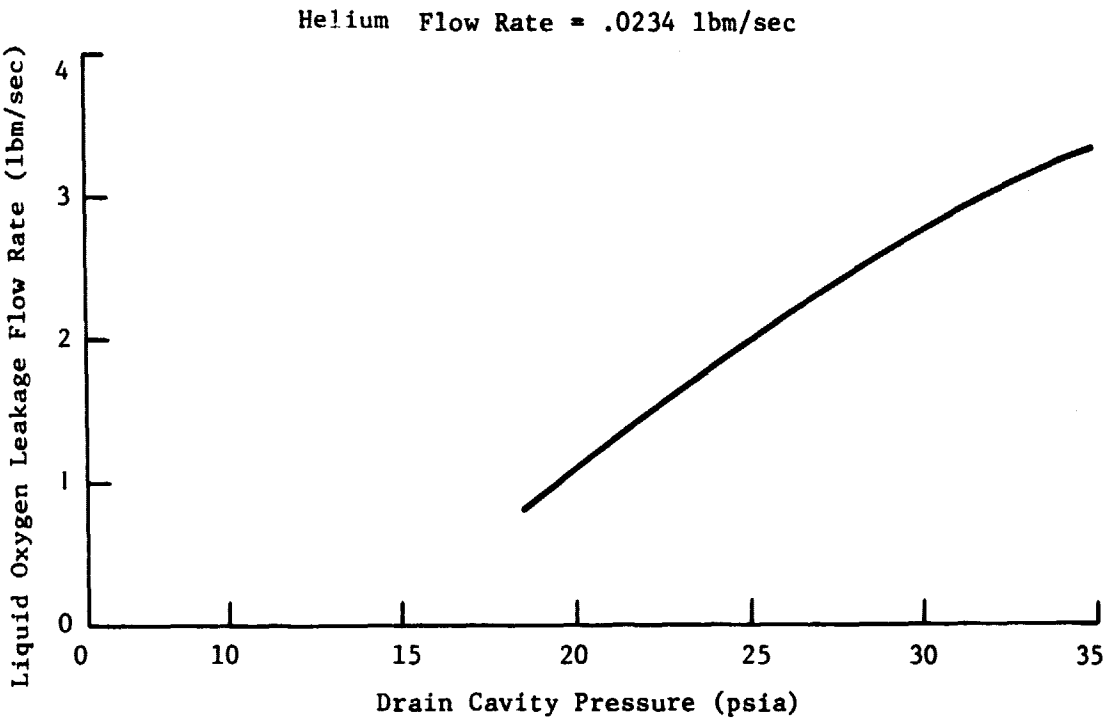

Fig. 3-11 HPOTP Turbine Bearing Coolant Model Coupled with Oxidizer Drain Resistance (with Leakage through the Bearing Support Bolt Holes)

REFERENCE FOR SECTION 3

3-1. Teal, G.A., "SSME Turbopump Flow Models - User's Manual," LMSC-HREC TR D867623, Lockheed Missiles & Space Company, Huntsville, Ala., October 1982.

4. SECOND STAGE HPFTP BLADE CRACK LENGTH STUDY

The objective of this study was to relate a statistical margin of safety to flow size in the second stage turbine blade of the HPFTP. The flow was defined as a crack in the aft edge of the blade shank, immediately under the platform. This crack was in the flow direction, through the shank, and of a variable length. The load conditions were power bending and centrifugal forces at 104 percent RPL. Thermal loads are not included, but thermal degradation of material properties were accounted for.

The method of analysis was to alter a finite element model of the subject blade (drawn from our existing library of models) by introducing a crack of varying length in the area of interest. An overall view of the model is shown in Fig. 4-1. A section of the critical area is shown in Fig. 4-2, with the discrete crack length investigated.

The resulting margins of safety are summarized in Table 4-1 and are presented graphically in Fig. 4-3.

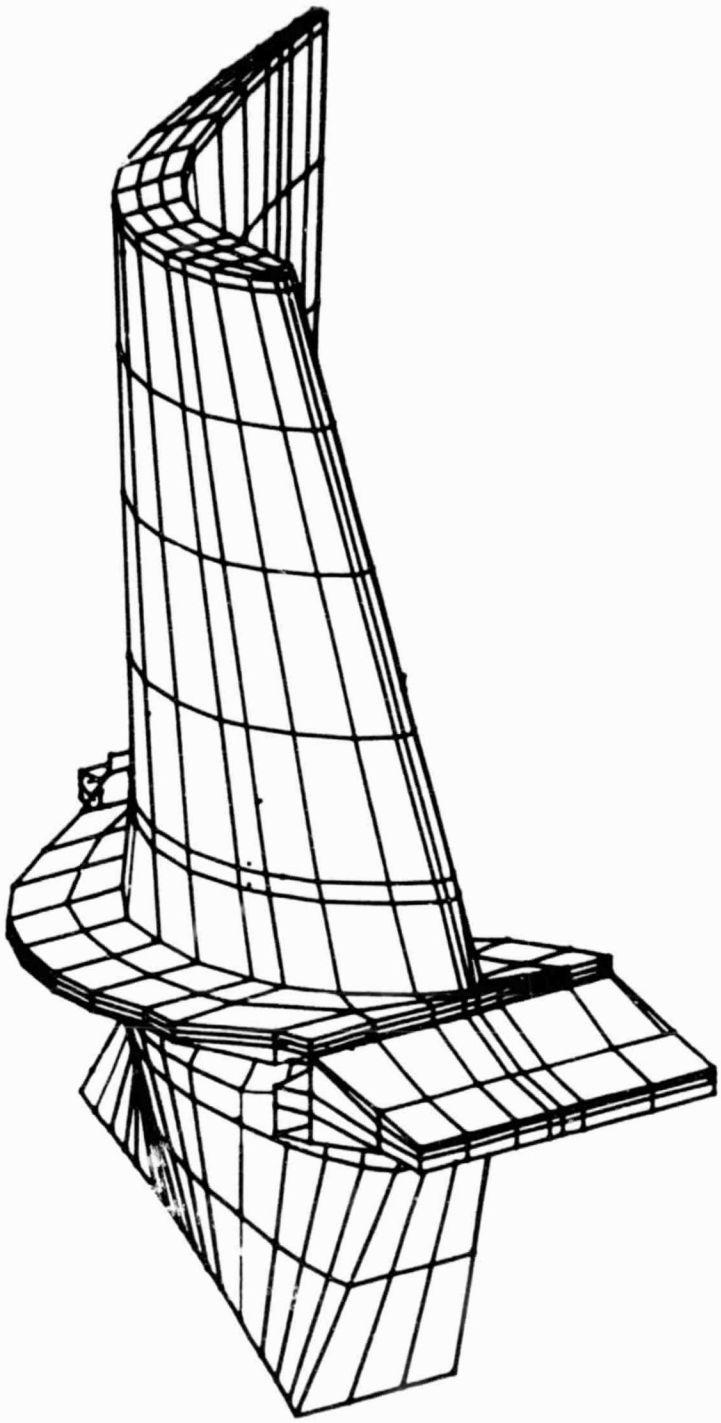

Fig. 4-1 HPFTP Second Stage Blade NASTRAN Model

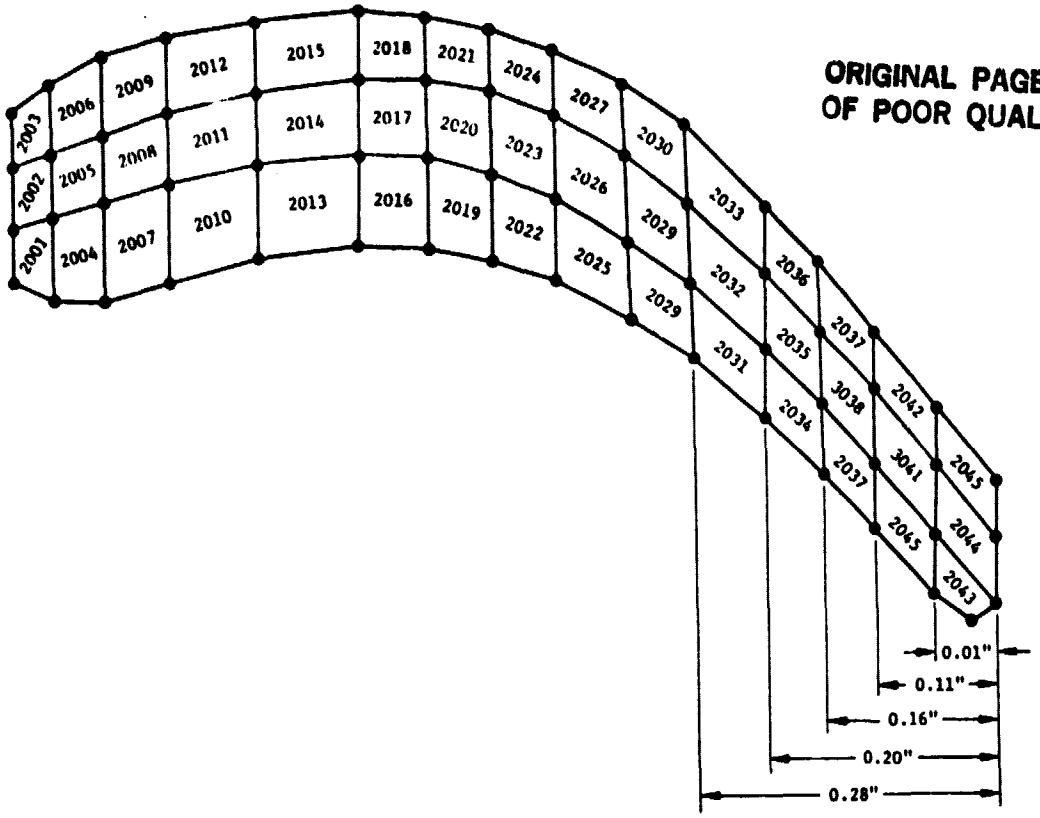

ORIGINAL PAGE IS
OF POOR QUALITY

Fig. 4-2 Critical Area and Crack Lengths

Table 4-1 STRESS AND FACTOR OF SAFETY AT VARIOUS CRACK LENGTHS

Crack Length (in.)	Tension Stress (ksi)	Bending Stress (ksi)	Factor of Safety
0.0	37.2	16.7	+2.05
0.01	41.9	21.3	+1.56
0.11	42.9	22.2	+1.50
0.16	57.2	36.6	+0.78
0.20	64.0	44.0	+0.36
0.28	94.9	78.1	-0.01

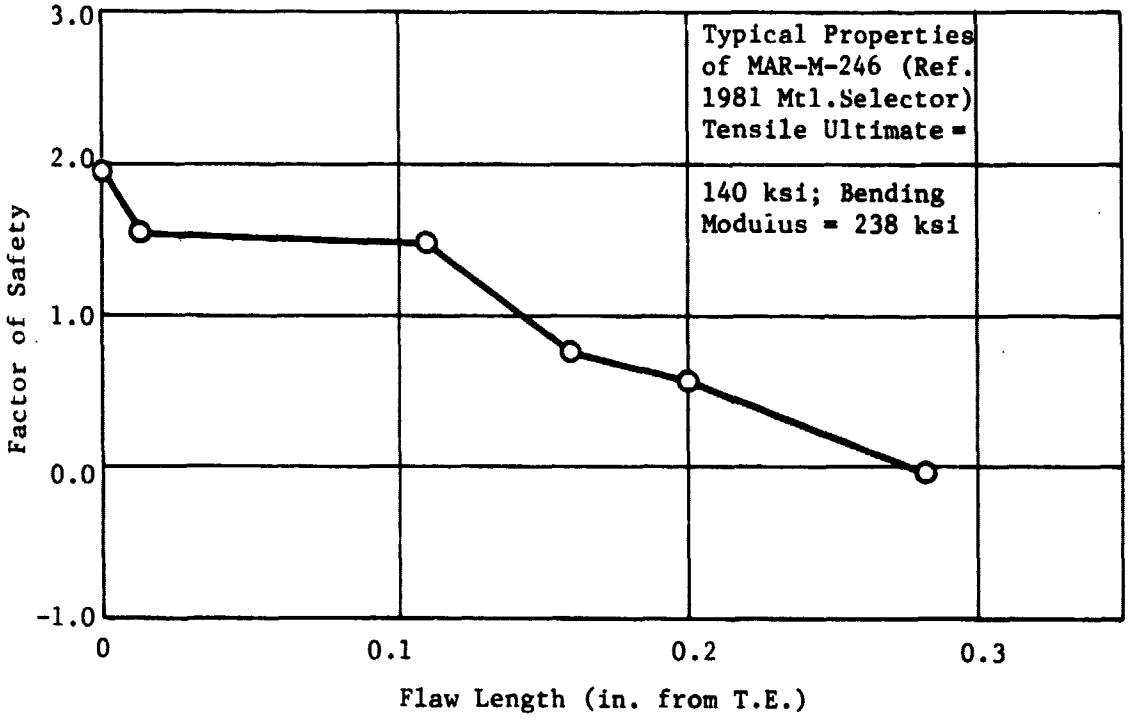

Fig. 4-3 Factor of Safety vs Crack Length HPFTP Second Stage Blade Shank at 104% RPL

5. HPFTP FIRST STAGE BLADE IMPACT STUDY

The objective of this study was to estimate the mass of a particle which would induce catastrophic failure of the first stage blade when encountered in the gas flow. This was accomplished by application of a BOPACE finite element model (drawn from our existing library of models) to perform an elastic-plastic energy balance solution. The method and results are detailed below.

5.1 METHOD OF ANALYSIS

Assuming that the particle is moving at the velocity of the gas stream prior to impact and does not affect the turbine speed upon impact, energy balance is written as follows:

v_g = gas velocity m_p = mass of particle

v_b = blade velocity U = strain energy

$$\frac{1}{2} m_p (v_g^2 - v_b^2) = U$$

The BOPACE plastic analysis program was used in the computation of the strain energy term, U. The failure criteria of $\varepsilon = 0.06$ is satisfied with a leading edge load of 2772 pounds (Fig. 5-1) which has a corresponding deflection of 0.198 in. at the point of application (Fig. 5-2). The strain energy is calculated by finding the area under the load deflection curve (Fig. 5-2) which yields:

$$U = \int_0^s F \cdot ds = 378.89 \text{ in.-lb.}$$

The following values were used in the energy balance equation:

v_g = 2493.6 ft/sec (HPFTP Turbine Flow Program)

v_b = 1649.1 ft/sec (FPL rotation at 10.19 diameter).

Inserting these values, and reducing:

$$m_p = \frac{2U}{(v_g^2 - v_b^2)}$$

$$m_p = \frac{2(379.89)}{(2493.6 \times 12)^2 - (1649.1 \times 12)^2}$$

$$m_p = 1.504 \times 10^{-6} \text{ lb/in./sec}^2$$

$$W_p = m_p (386) = 5.806 \times 10^{-4} \text{ lb.}$$

Assume a spherical shape and density of 0.3 lb/in^3:

$$V = \frac{W_p}{0.3} = 1.935 \times 10^{-3} \text{ in}^3.$$

$$d = 2 \left(\frac{3V}{4\pi F}\right)^{1/3} = .155 \text{ in. diameter}$$

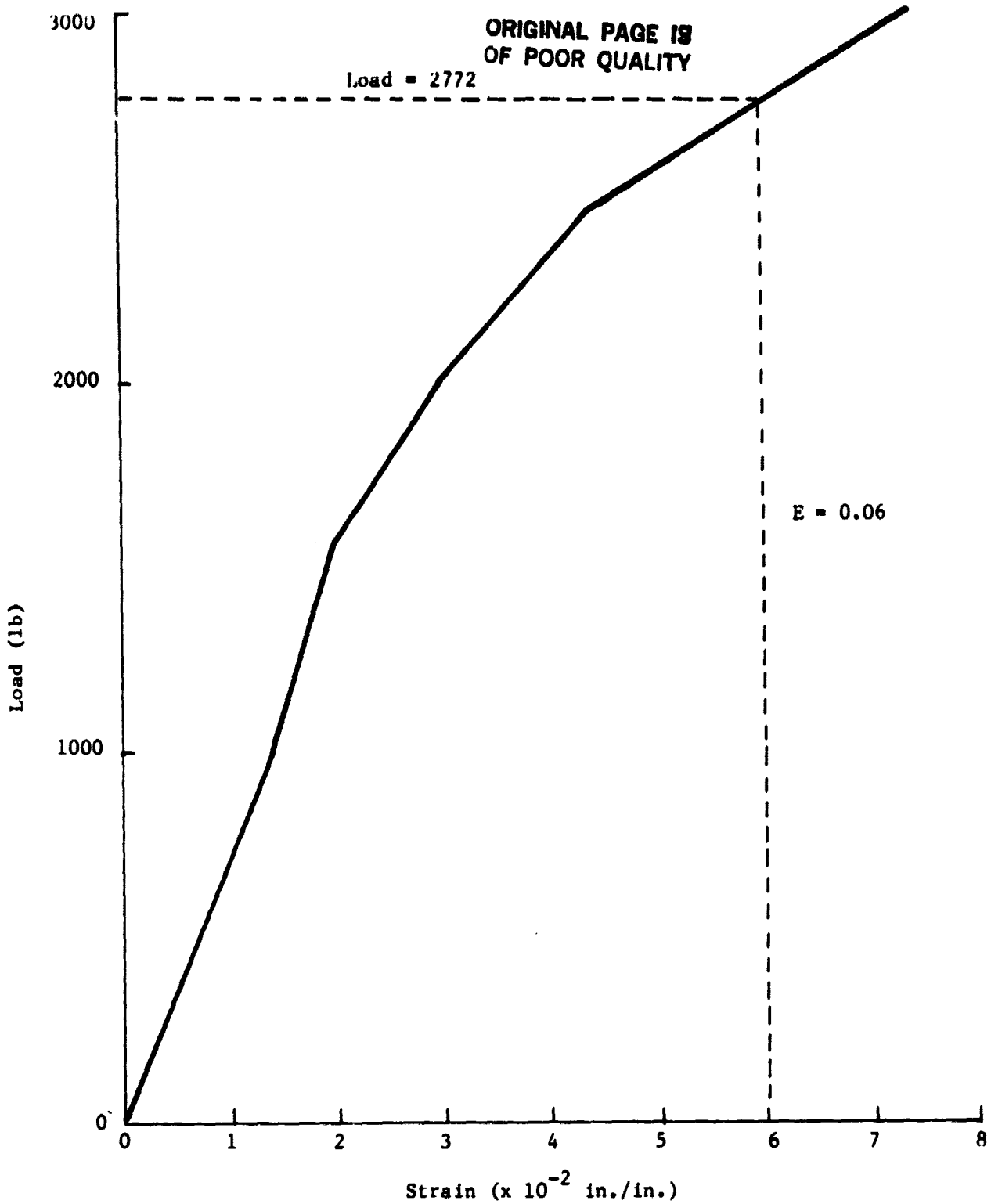

Fig. 5-1 Maximum Strain vs Applied Load

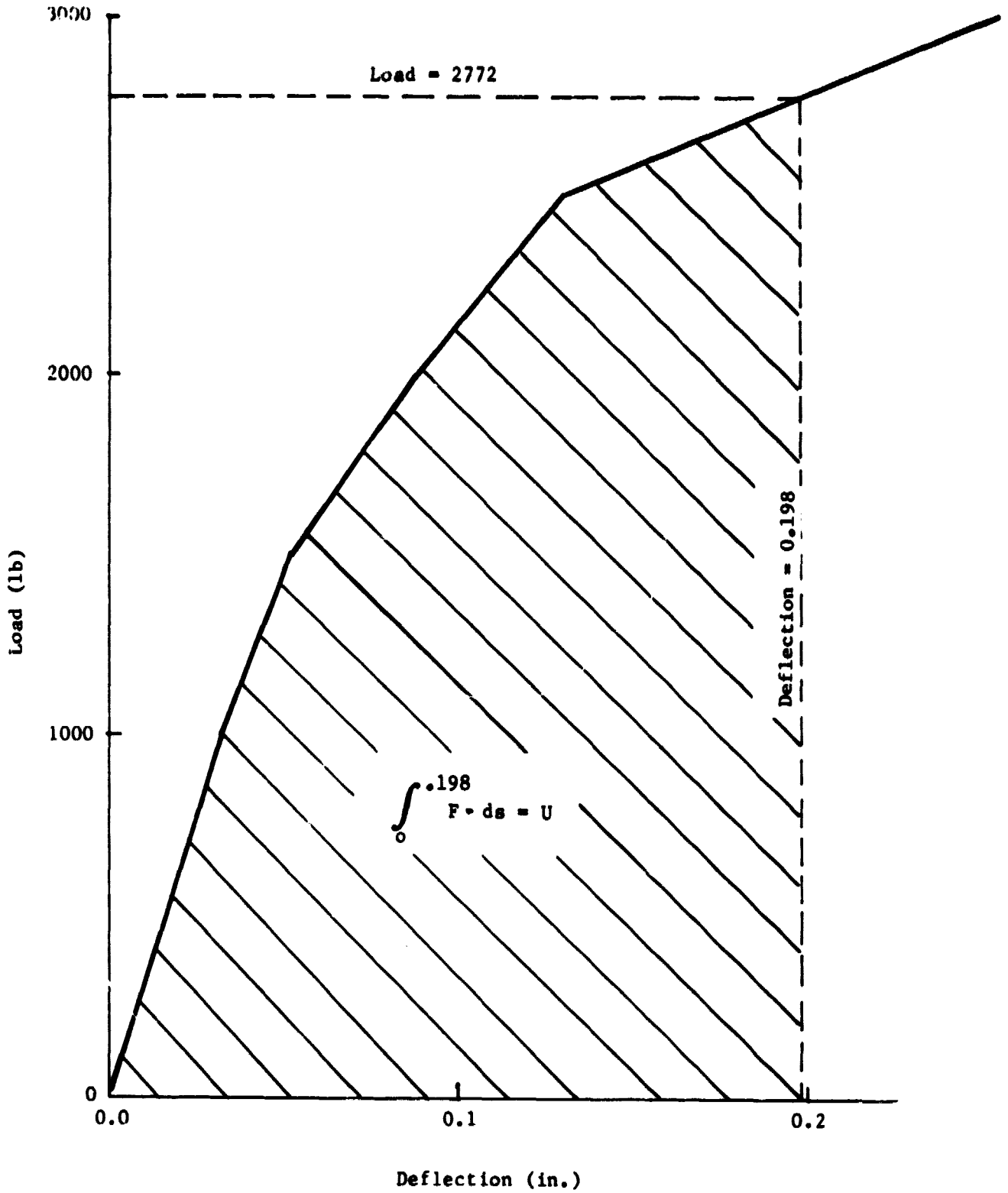

Fig. 5-2 Deflection at Leading Edge vs Applied Load